Biorthogonal cubic Hermite spline multiwavelets on the interval with complementary boundary conditions

Andreas Schneider*

October 31, 2007

In this article, a new biorthogonal multiwavelet basis on the interval with complementary homogeneous Dirichlet boundary conditions of second order is presented. This construction is based on the multiresolution analysis on $\mathbb{R}$ introduced in [DHJK00] which consists of cubic Hermite splines on the primal side.

Numerical results are given for the Riesz constants and both a non-adaptive and an adaptive discretization of the biharmonic equation, showing the superiority over other known boundary-adapted interval bases.

1 Introduction

Within the last years, wavelets have been successfully used for the numerical solution of PDEs. As many practical problems are formulated on domains $\Omega \subset \mathbb{R}^n$, corresponding bases are needed. Unfortunately, the construction of wavelet bases on domains is very difficult. The more general concept of wavelet frames, which allows for a *redundant* decomposition of functions, gives rise to much easier constructions. For instance, in [Ste03, DFR06] it has been shown that a frame on a domain can be obtained by a union of wavelet bases on subdomains, which in turn are lifted tensor products of a basis on the interval $[0, 1]$. Therefore, the properties of the employed interval wavelet basis are crucial for the properties of the resulting frame. Hence, well-conditioned interval bases are of great interest.

A biorthogonal wavelet basis, which in fact consists of two bases satisfying the biorthogonality relation, has the advantage that approximation order and vanishing moments can be imposed separately. It also gives rise to the possibility of complementary boundary conditions, i. e., the two biorthogonal bases have different boundary adaptations, allowing one of them to satisfy, e. g., Dirichlet boundary conditions, while the other one has free boundary conditions. This special kind of boundary adaptation has several benefits [DS98]. The most important one is that the dual basis reproduces polynomials on the whole interval; this ensures the primal boundary wavelets to have vanishing moments.

Several classical wavelet bases on the interval exist, e. g. the ones from [DS98, Pri06]. For piecewise linear and quadratic wavelets, the construction from [Pri06] is nearly optimal; however

* email: andreas@mathematik.uni-marburg.de

the numerical stability deteriorates for higher spline orders. In fact, for the numerical treatment of operator equations it is beneficial to work with cubic ansatz functions. For the construction of such a system with favorable numerical stability properties, we consider *multi*wavelet bases as an alternative. This concept, being more general than the classical approach, allows for an easy construction of cubic wavelet bases with short support and further desirable features like symmetry or interpolating properties.

For the conformal numerical discretization of fourth-order PDEs, suitable boundary conditions have to be incorporated into the ansatz functions. Concerning classical wavelet bases on the interval, such a boundary adaptation with complementary boundary conditions has been carried out in [DS98]. To the knowledge of the author, there is no corresponding result for multiwavelets. Anyway, there is a biorthogonal multiwavelet basis for the interval with free boundary conditions, published in [DHJK00]. In this approach there is still some freedom, so based on the multiresolution analysis on $\mathbb{R}$ from loc. cit., a new boundary adaptation with the desired complementary second-order Dirichlet boundary conditions has been carried out.

This article is structured as follows: In Section 2 the multiresolution analysis on $\mathbb{R}$ from [DHJK00] is shortly recalled. In Section 3 the new boundary adaptation for the MRA from Section 2 with complementary Dirichlet boundary conditions is given. For this MRA for $L_2(0,1)$, multiwavelets are constructed in Section 4 via stable completion. Some numerical results with this new multiwavelet basis are given in Section 5.

2 Multiresolution analysis on $\mathbb{R}$

This multiwavelet construction is based on the concept of multiresolution analysis, as most wavelet constructions are. In general, a multiresolution analysis for $L_2(\Omega), \Omega \subset \mathbb{R}$ is a sequence of closed subspaces $V_j \subset L_2(\Omega)$ which satisfy the following properties:

1. The spaces are nested,

$$V_j \subset V_{j+1} \quad \text{for all } j. \tag{2.1}$$

2. The sequence is asymptotically dense in $L_2(\Omega)$ and satisfies the separation property,

$$\begin{cases} \operatorname{clos}_{L_2} \bigcup_{j=-\infty}^{\infty} V_j = L_2(\mathbb{R}) \quad \text{and} \quad \bigcap_{j=-\infty}^{\infty} V_j = \{0\}, & \text{if } \Omega = \mathbb{R}, \\ \operatorname{clos}_{L_2} \bigcup_{j=j_0}^{\infty} V_j = L_2(\Omega), & \text{if } \Omega \subsetneq \mathbb{R}. \end{cases} \tag{2.2}$$

3. The spaces V_j are generated by the integer translates of the dilates of a finite number of generator functions $\varphi_1, \ldots, \varphi_r$, i. e.

$$V_j = \operatorname{clos}_{L_2} \operatorname{span}\{\varphi_i(2^j \cdot - k) : i \in \{1, \ldots, r\}, k \in \Delta_j\} \tag{2.3}$$

with the index set Δ_j.

Here we have $r = 2$. We begin with a pair of biorthogonal MRA on the real line $\mathbb{R}$ which are later adapted to the interval $[0,1]$. We use the MRA on $\mathbb{R}$ constructed in [DHJK00] which will be briefly summarized in the following.

2.1 The primal multigenerator

On the primal side, the multigenerator

$$\boldsymbol{\Phi} := \begin{pmatrix} \varphi_1 \\ \varphi_2 \end{pmatrix} \tag{2.4}$$

consists of cubic C^1 Hermite splines,

$$\varphi_1(x) := \begin{cases} (x+1)^2(-2x+1), & x \in [-1,0], \\ (1-x)^2(2x+1), & x \in [0,1], \\ 0, & \text{otherwise}, \end{cases} \qquad \varphi_2(x) := \begin{cases} (x+1)^2\, x, & x \in [-1,0], \\ (1-x)^2\, x, & x \in [0,1], \\ 0, & \text{otherwise}, \end{cases} \tag{2.5}$$

which fulfill the interpolation properties

$$\varphi_1(k) = \delta_{0,k}, \qquad \varphi_2'(k) = \delta_{0,k}, \qquad \varphi_1'(k) = 0, \qquad \varphi_2(k) = 0, \qquad \text{for all } k \in \mathbb{Z}, \tag{2.6}$$

where $\delta_{i,j}$ is the Kronecker delta. These functions are plotted in Figure 1. $\boldsymbol{\Phi}$ is *refinable*, i. e.

$$\boldsymbol{\Phi}(x) = \sum_{k \in \mathbb{Z}} \boldsymbol{A}_k \boldsymbol{\Phi}(2x-k) \tag{2.7}$$

with the mask

$$\boldsymbol{A}_{-1} = \begin{pmatrix} \frac{1}{2} & \frac{3}{4} \\ -\frac{1}{8} & -\frac{1}{8} \end{pmatrix}, \qquad \boldsymbol{A}_0 = \begin{pmatrix} 1 & 0 \\ 0 & \frac{1}{2} \end{pmatrix}, \qquad \boldsymbol{A}_1 = \begin{pmatrix} \frac{1}{2} & -\frac{3}{4} \\ \frac{1}{8} & -\frac{1}{8} \end{pmatrix}, \tag{2.8}$$

and $\boldsymbol{A}_k = \boldsymbol{0}$ for $k \notin \{-1,0,1\}$. It is also symmetric, meaning that the functions $\varphi_i, i \in \{1,2\}$ are either symmetric or antisymmetric; here, we have $\varphi_1(x) = \varphi_1(-x)$ and $\varphi_2(x) = -\varphi_2(-x)$ for all $x \in \mathbb{R}$. With the sign matrix

$$\boldsymbol{J} := \begin{pmatrix} 1 & 0 \\ 0 & -1 \end{pmatrix}, \tag{2.9}$$

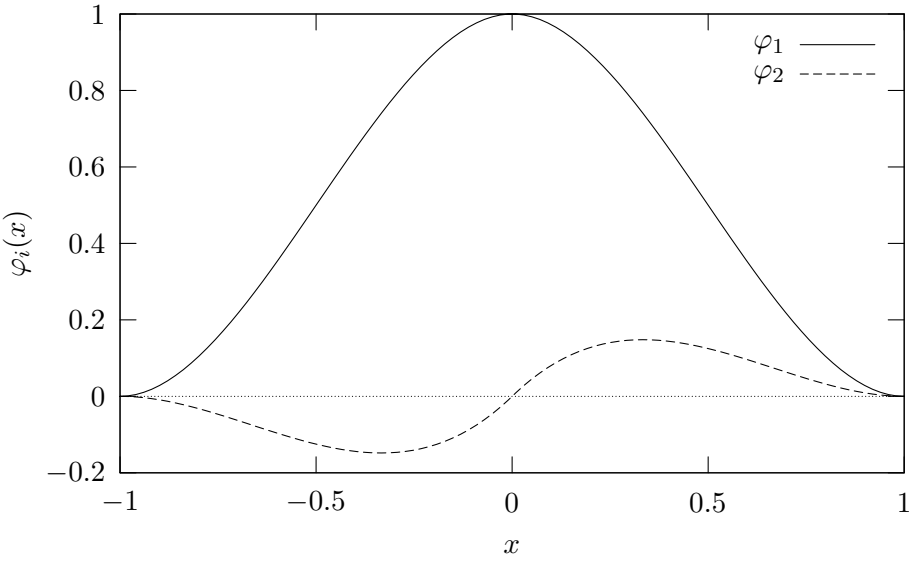

Figure 1: Components of the primal multigenerator $\boldsymbol{\Phi} = (\varphi_1, \varphi_2)^\top$ on $\mathbb{R}$

this symmetry relation can be written as

$$\boldsymbol{\Phi}(x) = \boldsymbol{J}\boldsymbol{\Phi}(-x) \quad \text{for all } x \in \mathbb{R}. \tag{2.10}$$

The symmetry of the generators transfers to the symbol in the sense that

$$\boldsymbol{A}_k = \boldsymbol{J}\boldsymbol{A}_{-k}\boldsymbol{J}, \quad k \in \mathbb{Z}. \tag{2.11}$$

The multigenerator is normalized such that

$$\int_{\mathbb{R}} \boldsymbol{\Phi}(x)\,\mathrm{d}x := \begin{pmatrix} \int_{\mathbb{R}} \varphi_1(x)\,\mathrm{d}x \\ \int_{\mathbb{R}} \varphi_2(x)\,\mathrm{d}x \end{pmatrix} = \begin{pmatrix} 1 \\ 0 \end{pmatrix}. \tag{2.12}$$

As a C^1 spline, $\boldsymbol{\Phi}$ is contained in the Sobolev space $(H^s(\mathbb{R}))^2$ for

$$s < \gamma := \frac{5}{2}. \tag{2.13}$$

Using the notation

$$\boldsymbol{f}_{(j,k)}(x) := 2^{j/2}\,\boldsymbol{f}(2^j x - k) := \begin{pmatrix} 2^{j/2}\,f_1(2^j x - k) \\ 2^{j/2}\,f_2(2^j x - k) \end{pmatrix} \tag{2.14}$$

to distinguish dilated and shifted quantities from the analogs defined on the interval, the spaces $V_j := \mathrm{clos}_{L_2}\,\mathrm{span}\{(\boldsymbol{\Phi}_{(j,k)})_i : i \in \{1,2\}, k \in \mathbb{Z}\}$ form a multiresolution analysis on $\mathbb{R}$ [DHJK00].

2.2 The dual multigenerator

Now we are looking for another compactly supported refinable function vector $\tilde{\boldsymbol{\Phi}} = (\tilde{\varphi}_1, \tilde{\varphi}_2)^\top$ which is *biorthogonal* to $\boldsymbol{\Phi}$, i. e.

$$\langle \boldsymbol{\Phi}, \tilde{\boldsymbol{\Phi}}(\cdot - k)\rangle_{\mathbb{R}} := (\langle \varphi_i(\cdot - k), \tilde{\varphi}_j(\cdot - k)\rangle_{\mathbb{R}})_{i,j=1}^2 = \delta_{0,k}\mathbf{I} \quad \text{for all } k \in \mathbb{Z}. \tag{2.15}$$

In order to find such a function, one first seeks a corresponding refinement mask $\tilde{\boldsymbol{A}}$ solving the discrete duality relation

$$\sum_{\ell \in \mathbb{Z}} \boldsymbol{A}_\ell \tilde{\boldsymbol{A}}_{\ell+2k}^\top = 2\delta_{0,k}\mathbf{I}, \quad \text{for all } k \in \mathbb{Z} \tag{2.16}$$

which is obtained by inserting the refinement equations (2.7) for the primal and the dual side into the biorthogonality relation (2.15). Here $\tilde{\boldsymbol{A}}$ is chosen to be

$$\begin{aligned} \tilde{\boldsymbol{A}}_{-2} &= \begin{pmatrix} -\frac{7}{64} & -\frac{5}{64} \\ \frac{87}{128} & \frac{31}{64} \end{pmatrix}, \quad \tilde{\boldsymbol{A}}_{-1} = \begin{pmatrix} \frac{1}{2} & \frac{3}{16} \\ -\frac{99}{32} & -\frac{37}{32} \end{pmatrix}, \quad \tilde{\boldsymbol{A}}_0 = \begin{pmatrix} \frac{39}{32} & 0 \\ 0 & \frac{15}{8} \end{pmatrix}, \\ \tilde{\boldsymbol{A}}_1 &= \begin{pmatrix} \frac{1}{2} & -\frac{3}{16} \\ \frac{99}{32} & -\frac{37}{32} \end{pmatrix}, \qquad \tilde{\boldsymbol{A}}_2 = \begin{pmatrix} -\frac{7}{64} & \frac{5}{64} \\ -\frac{87}{128} & \frac{31}{64} \end{pmatrix}, \quad \tilde{\boldsymbol{A}}_k = 0 \text{ for } k \notin \{-2, \dots, 2\}. \end{aligned} \tag{2.17}$$

In [DHJK00, Proposition 3.2] it is proven that there exists a unique function vector $\tilde{\boldsymbol{\Phi}} \in (L_2(\mathbb{R}))^2$ satisfying (2.16) which is refinable with the mask (2.17) and such that $\tilde{\boldsymbol{\Phi}} \in (H^s(\mathbb{R}))^2$ for any

$$s < \tilde{\gamma} := 0.824926\,. \tag{2.18}$$

The dual multigenerator is plotted in Figure 2. It is also proved in loc. cit. that with $\tilde{V}_j := \mathrm{clos}_{L_2}\,\mathrm{span}\{2^{j/2}\,(\tilde{\boldsymbol{\Phi}}_{(j,k)})_i : i \in \{1,2\}, k \in \mathbb{Z}\}$, $\tilde{\boldsymbol{\Phi}}$ generates a multiresolution analysis for $L_2(\mathbb{R})$ which is biorthogonal to (V_j).

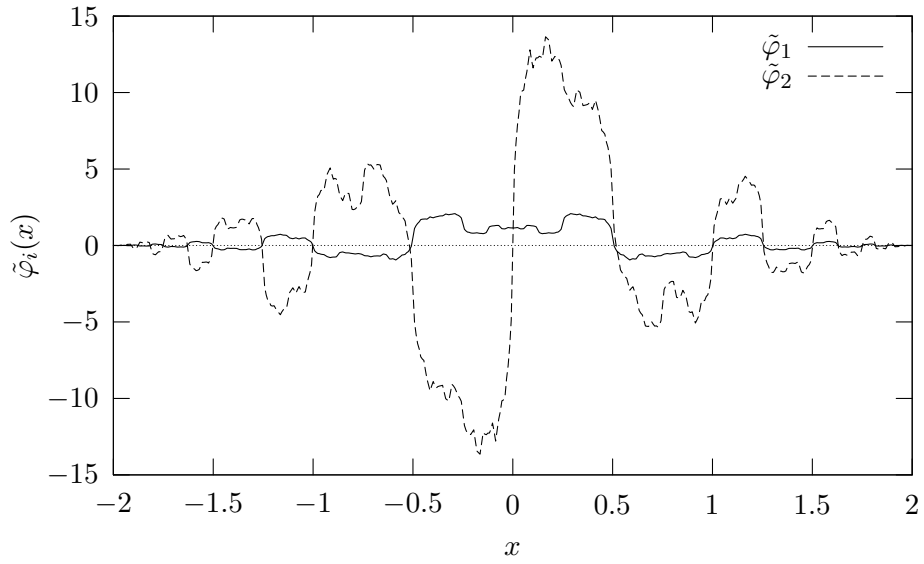

Figure 2: Components of the dual multigenerator $\tilde{\boldsymbol{\Phi}} = (\tilde{\varphi}_1, \tilde{\varphi}_2)^\top$ on $\mathbb{R}$

2.3 Polynomial exactness

Due to the interpolation properties of the Hermite cubic splines, the translates of the primal multigenerator $\boldsymbol{\Phi}$ reproduce polynomials up to the order

$$d := 4. \tag{2.19}$$

The dual generator reproduces polynomials of order

$$\tilde{d} := 2 \tag{2.20}$$

as shown in [DHJK00, Proposition 3.4]. For the dual moments

$$\tilde{\boldsymbol{\alpha}}_{k,m} := \int_{\mathbb{R}} x^m \, \tilde{\boldsymbol{\Phi}}(x-k) \, \mathrm{d}x := \begin{pmatrix} \int_{\mathbb{R}} x^m \, \tilde{\varphi}_1(x-k) \, \mathrm{d}x \\ \int_{\mathbb{R}} x^m \, \tilde{\varphi}_2(x-k) \, \mathrm{d}x \end{pmatrix} \in \mathbb{R}^2, \quad 0 \le m < d = 4, k \in \mathbb{Z}, \tag{2.21}$$

one obtains

$$\tilde{\boldsymbol{\alpha}}_{k,0} = \begin{pmatrix} 1 \\ 0 \end{pmatrix}, \qquad \tilde{\boldsymbol{\alpha}}_{k,1} = \begin{pmatrix} k \\ 1 \end{pmatrix}, \qquad \tilde{\boldsymbol{\alpha}}_{k,2} = \begin{pmatrix} k^2 \\ 2k \end{pmatrix}, \qquad \tilde{\boldsymbol{\alpha}}_{k,3} = \begin{pmatrix} k^3 \\ 3k^2 \end{pmatrix}, \qquad k \in \mathbb{Z}, \tag{2.22}$$

whereas the primal moments

$$\boldsymbol{\alpha}_{k,m} := \int_{\mathbb{R}} x^m \, \boldsymbol{\Phi}(x-k) \, \mathrm{d}x, \quad 0 \le m < \tilde{d} = 2, k \in \mathbb{Z} \tag{2.23}$$

are given by

$$\boldsymbol{\alpha}_{k,0} = \begin{pmatrix} 1 \\ 0 \end{pmatrix}, \quad \boldsymbol{\alpha}_{k,1} = \begin{pmatrix} k \\ \frac{1}{15} \end{pmatrix}, \quad k \in \mathbb{Z}. \tag{2.24}$$

They will be used later for the construction of the boundary-adapted functions.

3 Multiresolution analysis on [0, 1]

As second-order homogeneous Dirichlet boundary conditions are to be incorporated, a different boundary adaptation than that used in [DHJK00] is needed. The common strategy is to use as many translates as possible of the generators supported inside the interval and construct boundary functions for those generators that overlap the interval end, consisting of linear combinations of overlapping functions trimmed to the interval. The construction will be done on a minimal level j_0 which is chosen such that the boundary functions on the right and on the left do not overlap. In that way both ends of the interval can be treated separately. In our setting this is satisfied for $j_0 = 3$.

3.1 Boundary adaptation

Using the same index set as in [DHJK00],

$$\Delta_j := \{1, \dots, 2^j - 1\}, \tag{3.1}$$

we notice that no primal generator $\boldsymbol{\Phi}(2^j \cdot -k) = \boldsymbol{\Phi}_{(j,k)}, k \in \Delta_j$ overlaps the boundary, i. e. $\operatorname{supp} \boldsymbol{\Phi}_{(j,k)} \subset [0,1]$ for all $k \in \Delta_j$. Therefore, and because the primal generators fulfill the desired boundary condition, no boundary adaptation is needed on the primal side, and we can define

$$\boldsymbol{\Phi}_{j,k}(x) := 2^{j/2}\, \boldsymbol{\Phi}(2^j x - k), \quad k \in \Delta_j. \tag{3.2}$$

The primal generators at the base level $j = j_0 = 3$ are plotted in Figure 3.

As the same index set is wanted on the dual side, we define accordingly

$$\tilde{\Delta}_j := \Delta_j = \{1, \dots, 2^j - 1\}. \tag{3.3}$$

Unfortunately, $\tilde{\boldsymbol{\Phi}}_{(j,1)}$ and $\tilde{\boldsymbol{\Phi}}_{(j,2^j-1)}$ overlap the interval end, so indeed a boundary adaptation is needed. Defining

$$\tilde{\Delta}_j^{\mathrm{L}} := \{1\}, \qquad \tilde{\Delta}_j^{\mathrm{I}} := \{2, \dots, 2^j - 2\}, \qquad \tilde{\Delta}_j^{\mathrm{R}} := \{2^j - 1\} \tag{3.4}$$

as index sets for the left, inner and right function vectors, respectively, one has $\operatorname{supp} \tilde{\boldsymbol{\Phi}}_{(j,k)} \subset [0,1]$ for $k \in \tilde{\Delta}_j^{\mathrm{I}}$ and $\tilde{\Delta}_j^{\mathrm{L}} \cup \tilde{\Delta}_j^{\mathrm{I}} \cup \tilde{\Delta}_j^{\mathrm{R}} = \tilde{\Delta}_j$. Note that $\#(\tilde{\Delta}_j^{\mathrm{L}} \cup \tilde{\Delta}_j^{\mathrm{R}}) = 2 = \tilde{d}$ which is equal to the order of polynomial exactness of $\tilde{\boldsymbol{\Phi}}$. Since free boundary conditions are desired on the dual side, the same preliminary (i. e. before biorthogonalization) boundary functions as in [DHJK00] can be used. These functions are chosen such that they are furthermore refinable; the definition is motivated by the following lemma [DHJK00, Lemma 4.2] which is proved in [DKU99, Lemma 3.1]:

Lemma 3.1. *Suppose that $\boldsymbol{\Theta}$ and $\tilde{\boldsymbol{\Theta}}$ form a pair of dual refinable multigenerators with $\operatorname{supp} \tilde{\boldsymbol{\Theta}} =: [-\tilde{\lambda}, \tilde{\lambda}]$, and that $\tilde{\boldsymbol{\Theta}}$ is exact of order $\tilde{d}$. Let $\tilde{\boldsymbol{A}} = (\tilde{\boldsymbol{A}}_k)_{k=-\tilde{\lambda}}^{\tilde{\lambda}}$ denote the mask of $\tilde{\boldsymbol{\Theta}}$ satisfying $\operatorname{supp} \tilde{\boldsymbol{A}} = \{-\tilde{\lambda}, \dots, \tilde{\lambda}\}$. Let $\ell \geq \tilde{\lambda}$ and define*

$$\boldsymbol{\alpha}_{\boldsymbol{\Theta},m}(k) := \int_{\mathbb{R}} x^m \boldsymbol{\Theta}(x-k)\, \mathrm{d}x, \tag{3.5}$$

$$\tilde{\vartheta}_{j,m}^{\mathrm{L}} := \sum_{k=-\tilde{\lambda}+1}^{\ell-1} \boldsymbol{\alpha}_{\boldsymbol{\Theta},m}(k)^\top \tilde{\boldsymbol{\Theta}}_{(j,k)}|_{\mathbb{R}^+}, \quad m = 0, \dots, \tilde{d} - 1. \tag{3.6}$$

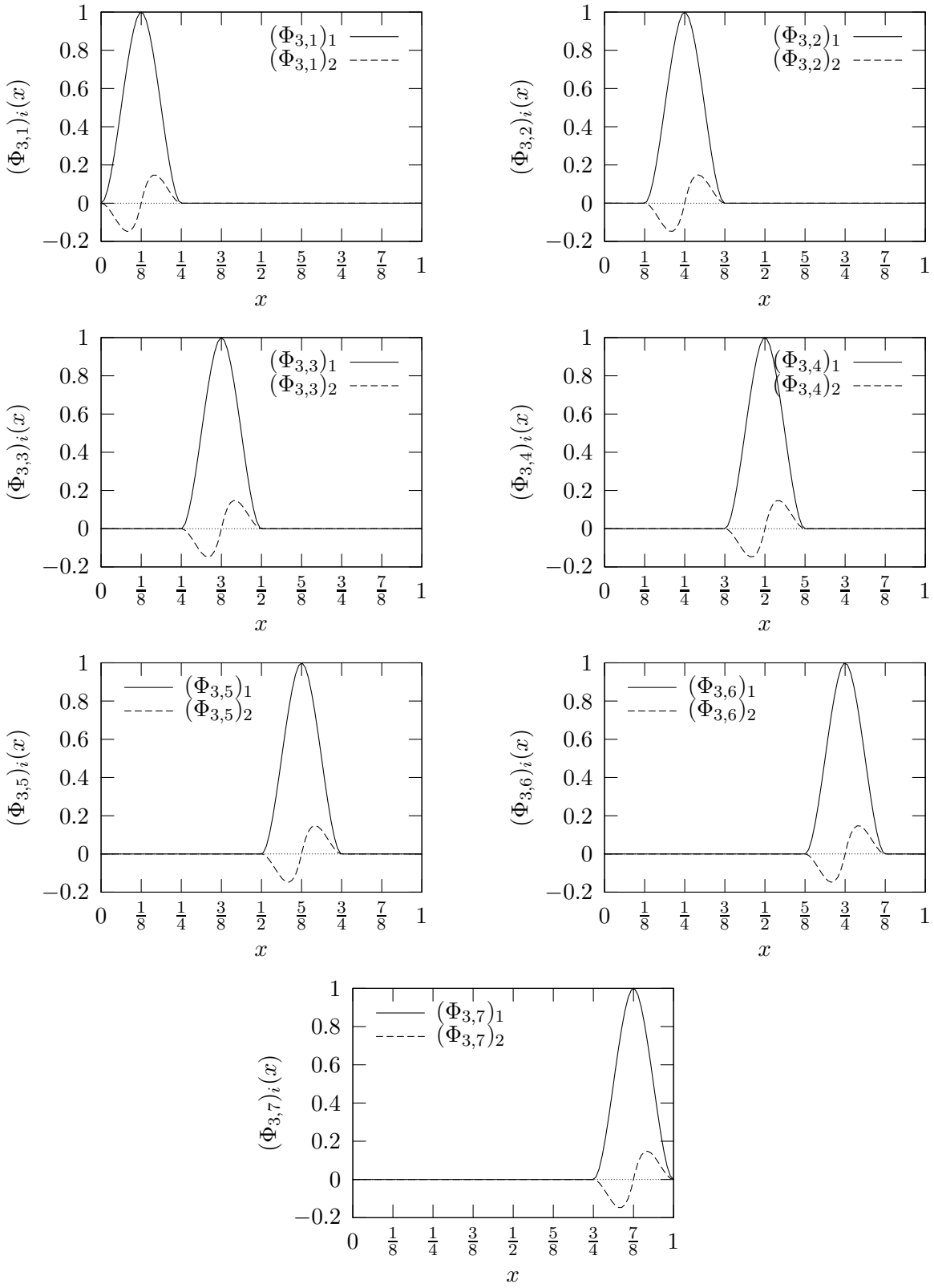

Figure 3: Components of the primal multigenerators $\mathbf{\Phi}_{3,k}, k \in \Delta_3 = \{1, \ldots, 7\}$, on the base level

Then with

$$\boldsymbol{\beta}_{\boldsymbol{\Theta},m}(k)^\top := 2^{-\frac{1}{2}} \sum_{q=\lceil (k-\tilde{\lambda})/2 \rceil}^{\ell-1} \boldsymbol{\alpha}_{\boldsymbol{\Theta},m}(q)^\top \tilde{\boldsymbol{A}}_{k-2q}, \tag{3.7}$$

one has

$$\tilde{\vartheta}^{\mathrm{L}}_{j,m} = 2^{-(m+\frac{1}{2})} \left(\tilde{\vartheta}^{\mathrm{L}}_{j+1,m} + \sum_{k=\ell}^{2\ell-\tilde{\lambda}-1} \boldsymbol{\alpha}_{\boldsymbol{\Theta},m}(k)^\top \tilde{\boldsymbol{\Theta}}_{(j+1,k)} \right) + \sum_{k=2\ell-\tilde{\lambda}}^{2\ell+\tilde{\lambda}-2} \boldsymbol{\beta}_{\boldsymbol{\Theta},m}(k)^\top \tilde{\boldsymbol{\Theta}}_{(j+1,k)}, \quad m = 0, \dots, \tilde{d}-1. \tag{3.8}$$

Having this lemma in mind, we define the (dual) functions on the left end of the interval to be

$$\tilde{\eta}^{\mathrm{L}}_{j,m}(x) := \sum_{k=-1}^{1} \boldsymbol{\alpha}^\top_{k,m} \tilde{\boldsymbol{\Phi}}_{(j,k)}(x)|_{[0,1]}, \quad m = 0, 1 \tag{3.9}$$

which are collected in a vector

$$\tilde{\boldsymbol{\Phi}}^{\mathrm{L},\vee}_{j,1} := \begin{pmatrix} \tilde{\eta}^{\mathrm{L}}_{j,0} \\ \tilde{\eta}^{\mathrm{L}}_{j,1} \end{pmatrix}. \tag{3.10}$$

The notation $\vee$ indicates that these functions are still preliminary (they are not yet biorthogonal) and will have to be modified later on.

For the right end of the interval we use symmetry

$$\tilde{\boldsymbol{\Phi}}_{(j,k)}(1-x) = \boldsymbol{J} \tilde{\boldsymbol{\Phi}}_{(j,2^j-k)}(x) \tag{3.11}$$

with $\boldsymbol{J}$ from (2.9). With

$$\boldsymbol{\alpha}^{\mathrm{R}}_{j,k,m} := -\int_{\mathbb{R}} (2^j - x)^m \boldsymbol{\Phi}(x-k)\,\mathrm{d}x = \boldsymbol{J} \boldsymbol{\alpha}_{2^j-k,m} \tag{3.12}$$

we define

$$\tilde{\eta}^{\mathrm{R}}_{j,2^j-m}(x) := \sum_{k=2^j-1}^{2^j+1} (\boldsymbol{\alpha}^{\mathrm{R}}_{j,k,m})^\top \tilde{\boldsymbol{\Phi}}_{(j,k)}(x)|_{[0,1]}, \quad m = 0, 1. \tag{3.13}$$

It is easy to see from the definition that we have the symmetry relation

$$\begin{aligned} \tilde{\eta}^{\mathrm{R}}_{j,2^j-m}(1-x) &= \sum_{k=2^j-1}^{2^j+1} \boldsymbol{\alpha}^\top_{2^j-k,m} \boldsymbol{J} \tilde{\boldsymbol{\Phi}}_{(j,k)}(1-x)|_{[0,1]} \\ &= \tilde{\eta}^{\mathrm{L}}_{j,m}(x), \quad m = 0, 1, \quad x \in [0,1]. \end{aligned} \tag{3.14}$$

The functions on the right end are also collected in a vector

$$\tilde{\boldsymbol{\Phi}}^{\mathrm{R},\vee}_{j,2^j-1} := \begin{pmatrix} \tilde{\eta}^{\mathrm{R}}_{j,2^j-1} \\ \tilde{\eta}^{\mathrm{R}}_{j,2^j} \end{pmatrix}. \tag{3.15}$$

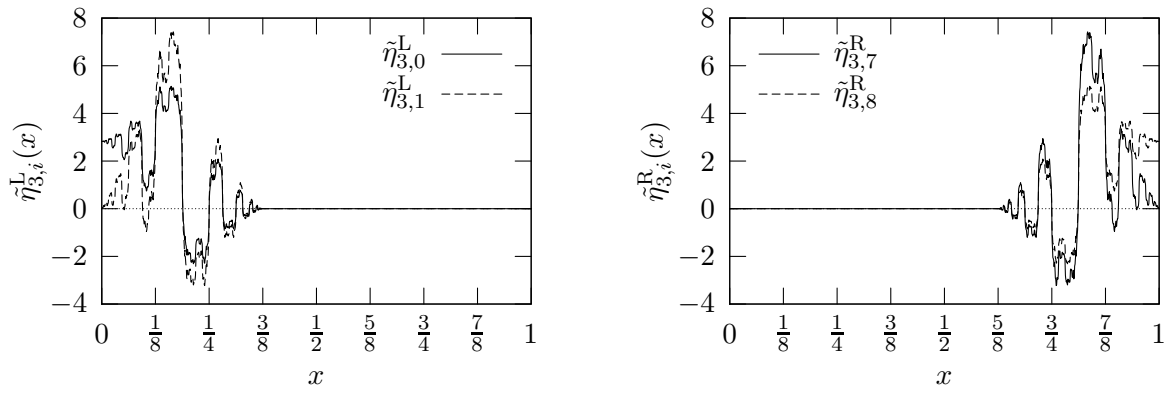

Figure 4: Boundary-adapted generators $\tilde{\boldsymbol{\Phi}}^{\mathrm{L},\vee}_{j,1}$, $\tilde{\boldsymbol{\Phi}}^{\mathrm{R},\vee}_{j,2^j-1}$, on the base level before biorthogonalization

The (preliminary) boundary-adapted functions are plotted in Figure 4.

Now we have a first set of multigenerators. The generators of one level are collected in a large vector,

$$\Phi_j := \left(\boldsymbol{\Phi}^\top_{j,1}, \ldots, \boldsymbol{\Phi}^\top_{j,2^j-2}\right)^\top \tag{3.16}$$

on the primal side and

$$\tilde{\Phi}^{\mathrm{L},\vee}_j := \tilde{\boldsymbol{\Phi}}^{\mathrm{L},\vee}_{j,1}, \qquad \tilde{\Phi}^{\mathrm{I}}_j := \left(\tilde{\boldsymbol{\Phi}}^\top_{(j,2)}, \ldots, \tilde{\boldsymbol{\Phi}}^\top_{(j,2^j-2)}\right)^\top, \qquad \tilde{\Phi}^{\mathrm{R},\vee}_j := \tilde{\boldsymbol{\Phi}}^{\mathrm{R},\vee}_{j,2^j-1}, \tag{3.17}$$

$$\tilde{\Phi}^\vee_j := \left((\tilde{\Phi}^{\mathrm{L},\vee}_j)^\top, (\tilde{\Phi}^{\mathrm{I}}_j)^\top, (\tilde{\Phi}^{\mathrm{R},\vee}_j)^\top\right)^\top \tag{3.18}$$

on the dual side.

3.2 Refinement equations

In this subsection the refinement equation for the (preliminary) boundary-adapted multigenerators are derived. These relations will be written in matrix-vector form.

On the primal side no boundary adaptation is done, so we still have the refinement relation (2.7) with the mask (2.8). In matrix-vector form, this is written as

$$\Phi^\top_j = \Phi^\top_{j+1} \boldsymbol{M}_{j,0} \tag{3.19}$$

with the coefficient matrix

$$\boldsymbol{M}_{j,0} = \frac{1}{\sqrt{2}} \begin{pmatrix} \boldsymbol{A}_{-1} & & & \\ \boldsymbol{A}_0 & & & \\ \boldsymbol{A}_1 & \boldsymbol{A}_{-1} & & \\ & \boldsymbol{A}_0 & & \\ & \boldsymbol{A}_1 & \ddots & \boldsymbol{A}_{-1} \\ & & & \boldsymbol{A}_0 \\ & & & \boldsymbol{A}_1 \end{pmatrix} \tag{3.20}$$

and $\boldsymbol{A}$ from (2.8).

On the dual side, the preliminary boundary-adapted functions $\tilde{\Phi}_j^\vee$ defined in (3.18) satisfy the refinement equation

$$(\tilde{\Phi}_j^\vee)^\top = (\tilde{\Phi}_{j+1}^\vee)^\top \tilde{\boldsymbol{M}}_{j,0}^\vee \tag{3.21}$$

with

$$\tilde{\boldsymbol{M}}_{j,0}^\vee := \begin{pmatrix} \tilde{\boldsymbol{M}}_{\mathrm{L}}^\vee & & 0 \\ & \tilde{\boldsymbol{M}}_{j,0}^{\mathrm{I}} & \\ 0 & & \tilde{\boldsymbol{M}}_{\mathrm{R}}^\vee \end{pmatrix} \in \mathbb{R}^{2(\Delta_{j+1}\times\Delta_j)}. \tag{3.22}$$

and the block matrices $\tilde{\boldsymbol{M}}_{j,0}^{\mathrm{I}}, \tilde{\boldsymbol{M}}_{\mathrm{R}}^\vee, \tilde{\boldsymbol{M}}_{\mathrm{L}}^\vee$. As the inner functions are not modified, the interior block matrix $\tilde{\boldsymbol{M}}_{j,0}^{\mathrm{I}}$ has the form

$$(\tilde{\boldsymbol{M}}_{j,0}^{\mathrm{I}})_{k,m} := \frac{1}{\sqrt{2}} \tilde{\boldsymbol{A}}_{k-2m}^\top, \quad k \in \tilde{\Delta}_{j+1}^{\mathrm{I}}, m \in \tilde{\Delta}_j^{\mathrm{I}} \tag{3.23}$$

with $\tilde{\boldsymbol{A}}$ from (2.17). Note that only the size of $\tilde{\boldsymbol{M}}_{j,0}^{\mathrm{I}}$ depends on j, but neither its band width nor its entries. For the description of the boundary blocks, recall Lemma 3.1. According to (3.7), we define

$$\boldsymbol{\beta}_{k,m}^\top := 2^{-1/2} \sum_{q=\lceil (k-2)/2 \rceil}^{1} \boldsymbol{\alpha}_{q,m}^\top \tilde{\boldsymbol{A}}_{k-2q}. \tag{3.24}$$

The actual values of these coefficients are given in Table 1. For the right end of the interval, the coefficients

$$(\boldsymbol{\beta}_{j,k,m}^{\mathrm{R}})^\top := 2^{-1/2} \sum_{q=2^j-1}^{2^j-\lceil (k-2)/2 \rceil} (\boldsymbol{\alpha}_{j,q,m}^{\mathrm{R}})^\top \tilde{\boldsymbol{A}}_{2^{j+1}-k-2q} \boldsymbol{J} \tag{3.25}$$

are obtained by the symmetry relation $\boldsymbol{\beta}_{j,k,m}^{\mathrm{R}} = \boldsymbol{\beta}_{2^{j+1}-k,m}$. Using (3.8) in matrix-vector form,

k \ m	2	3	4
0	$\begin{pmatrix} \frac{71}{64\sqrt{2}} \\ \frac{5}{64\sqrt{2}} \end{pmatrix}$	$\begin{pmatrix} \frac{1}{2\sqrt{2}} \\ -\frac{3}{16\sqrt{2}} \end{pmatrix}$	$\begin{pmatrix} -\frac{7}{64\sqrt{2}} \\ \frac{5}{64\sqrt{2}} \end{pmatrix}$
1	$\begin{pmatrix} \frac{2253}{128\cdot 15\sqrt{2}} \\ \frac{151}{64\cdot 15\sqrt{2}} \end{pmatrix}$	$\begin{pmatrix} \frac{339}{32\cdot 15\sqrt{2}} \\ -\frac{127}{32\cdot 15\sqrt{2}} \end{pmatrix}$	$\begin{pmatrix} -\frac{297}{128\cdot 15\sqrt{2}} \\ \frac{106}{64\cdot 15\sqrt{2}} \end{pmatrix}$

Table 1: Values of $\boldsymbol{\beta}_{k,m},\ k = 0, 1,\ m = 2, 3, 4$

the boundary blocks are given by

$$\tilde{\boldsymbol{M}}_{\mathrm{L}}^{\vee} := \begin{pmatrix} 2^{-1/2} & \\ & 2^{-3/2} \\ \boldsymbol{\beta}_{2,0} & \boldsymbol{\beta}_{2,1} \\ \boldsymbol{\beta}_{3,0} & \boldsymbol{\beta}_{3,1} \\ \boldsymbol{\beta}_{4,0} & \boldsymbol{\beta}_{4,1} \end{pmatrix} =: \begin{pmatrix} \tilde{\boldsymbol{D}}_{\mathrm{L}} \\ \tilde{\boldsymbol{B}}_{\mathrm{L}} \end{pmatrix} \in \begin{cases} \mathbb{R}^{2\times 2} \\ \mathbb{R}^{6\times 2} \end{cases} \tag{3.26}$$

and

$$\tilde{\boldsymbol{M}}_{\mathrm{R}}^{\vee} := \begin{pmatrix} \boldsymbol{J}\boldsymbol{\beta}^{\mathrm{R}}_{j,2^{j+1}-4,1} & \boldsymbol{J}\boldsymbol{\beta}^{\mathrm{R}}_{j,2^{j+1}-4,0} \\ \boldsymbol{J}\boldsymbol{\beta}^{\mathrm{R}}_{j,2^{j+1}-3,1} & \boldsymbol{J}\boldsymbol{\beta}^{\mathrm{R}}_{j,2^{j+1}-3,0} \\ \boldsymbol{J}\boldsymbol{\beta}^{\mathrm{R}}_{j,2^{j+1}-2,1} & \boldsymbol{J}\boldsymbol{\beta}^{\mathrm{R}}_{j,2^{j+1}-2,0} \\ 2^{-3/2} & \\ & 2^{-1/2} \end{pmatrix} =: \begin{pmatrix} \tilde{\boldsymbol{B}}_{\mathrm{R}} \\ \tilde{\boldsymbol{D}}_{\mathrm{R}} \end{pmatrix} \in \begin{cases} \mathbb{R}^{6\times 2} \\ \mathbb{R}^{2\times 2} \end{cases} . \tag{3.27}$$

3.3 Biorthogonalization

The boundary functions are not yet biorthogonal with respect to $\langle\cdot,\cdot\rangle_{L_2(0,1)}$. To remedy of this fact, a linear transformation is applied to the dual functions. We proceed as in [Pri06, Section 2.5]. Since the inner generators are dilated and translated versions of $\tilde{\boldsymbol{\Phi}}$, they are already biorthogonal, so we have to transform only locally near the boundary. On the left end we want to do a transformation

$$\tilde{\Phi}_j^{\mathrm{L}} := \tilde{\boldsymbol{C}}_{\mathrm{L}}\, \tilde{\Phi}_j^{\mathrm{L},\vee} \tag{3.28}$$

with the coefficient matrix $\tilde{\boldsymbol{C}}_{\mathrm{L}} \in \mathbb{R}^{2\times 2}$, such that the new functions fulfill the biorthogonality relation

$$\langle \Phi_j^{\mathrm{L}}, \tilde{\Phi}_j^{\mathrm{L}} \rangle_{[0,1]} = \mathbf{I}_2. \tag{3.29}$$

Inserting (3.28) into (3.29), it follows that

$$\tilde{\boldsymbol{C}}_{\mathrm{L}} = \langle \Phi_j^{\mathrm{L}}, \tilde{\Phi}_j^{\mathrm{L},\vee} \rangle_{[0,1]}^{-\top}. \tag{3.30}$$

The Gramian matrix $\boldsymbol{\Gamma}_{\mathrm{L}} := \langle \Phi_j^{\mathrm{L}}, \tilde{\Phi}_j^{\mathrm{L},\vee} \rangle_{[0,1]}$ is calculated in the way introduced in [Pri06, p. 39]. Using the refinement equation, with the boundary blocks $\tilde{\boldsymbol{D}}_{\mathrm{L}}, \tilde{\boldsymbol{B}}_{\mathrm{L}}$ from (3.26) and the analogs for the right end

$$\boldsymbol{D}_{\mathrm{L}} := \boldsymbol{A}_{-1}^{\top} \in \mathbb{R}^{2\times 2}, \quad \boldsymbol{B}_{\mathrm{L}} := \begin{pmatrix} \boldsymbol{A}_0^{\top} \\ \boldsymbol{A}_1^{\top} \\ \mathbf{0} \end{pmatrix} \in \mathbb{R}^{6\times 2}$$

(which are artificially understood as boundary blocks here), one has

$$\begin{aligned} \boldsymbol{\Gamma}_{\mathrm{L}} = \langle \Phi_j^{\mathrm{L}}, \tilde{\Phi}_j^{\mathrm{L}} \rangle_{[0,1]} &= \int_0^1 \Phi_j^{\mathrm{L}}(x) (\tilde{\Phi}_j^{\mathrm{L}}(x))^{\top}\, \mathrm{d}x = \int_0^1 \boldsymbol{M}_{\mathrm{L}}^{\top} \begin{pmatrix} \Phi_{j+1}^{\mathrm{L}}(x) \\ \Phi_{j+1}^{\mathrm{I}}(x) \end{pmatrix} \begin{pmatrix} \tilde{\Phi}_{j+1}^{\mathrm{L}}(x) \\ \tilde{\Phi}_{j+1}^{\mathrm{I}}(x) \end{pmatrix}^{\top} \tilde{\boldsymbol{M}}_{\mathrm{L}}\, \mathrm{d}x \\ &= (\boldsymbol{D}_{\mathrm{L}}^{\top}, \boldsymbol{B}_{\mathrm{L}}^{\top}) \int_0^1 \begin{pmatrix} \Phi_{j+1}^{\mathrm{L}}(x) \\ \Phi_{j+1}^{\mathrm{I}}(x) \end{pmatrix} \begin{pmatrix} \tilde{\Phi}_{j+1}^{\mathrm{L}}(x) \\ \tilde{\Phi}_{j+1}^{\mathrm{I}}(x) \end{pmatrix}^{\top} \mathrm{d}x \begin{pmatrix} \tilde{\boldsymbol{D}}_{\mathrm{L}} \\ \tilde{\boldsymbol{B}}_{\mathrm{L}} \end{pmatrix}. \end{aligned} \tag{3.31}$$

Using the fact that the inner functions are already biorthogonal, one obtains

$$\boldsymbol{\Gamma}_{\mathrm{L}} = (\boldsymbol{D}_{\mathrm{L}}^{\top}, \boldsymbol{B}_{\mathrm{L}}^{\top}) \begin{pmatrix} \boldsymbol{\Gamma}_{\mathrm{L}} & \mathbf{0} \\ \mathbf{0} & \mathbf{I} \end{pmatrix} \begin{pmatrix} \tilde{\boldsymbol{D}}_{\mathrm{L}} \\ \tilde{\boldsymbol{B}}_{\mathrm{L}} \end{pmatrix} = \boldsymbol{D}_{\mathrm{L}}^{\top} \boldsymbol{\Gamma}_{\mathrm{L}} \tilde{\boldsymbol{D}}_{\mathrm{L}} + \boldsymbol{B}_{\mathrm{L}}^{\top} \tilde{\boldsymbol{B}}_{\mathrm{L}}. \tag{3.32}$$

Defining the linear invertible mapping

$$\mathrm{col} : \mathbb{R}^{n \times n} \to \mathbb{R}^{n^2}, (a_1, \ldots, a_n) \mapsto (a_1^{\top}, \ldots, a_n^{\top})^{\top},$$

with the Kronecker product

$$\otimes : \mathbb{R}^{n \times m} \times \mathbb{R}^{s \times t} \to \mathbb{R}^{ns \times mt}, (A \otimes B) := (a_{ij}\, B)_{i,j=1}^{n,m} = \begin{pmatrix} a_{11}B & \cdots & a_{1n}B \\ \vdots & \ddots & \vdots \\ a_{m1}B & \cdots & a_{mn}B \end{pmatrix},$$

we have

$$(\mathbf{I}_{2^2} - \tilde{\boldsymbol{D}}_{\mathrm{L}}^{\top} \otimes \boldsymbol{D}_{\mathrm{L}})\, \gamma_{\mathrm{L}} = \mathrm{col}(\boldsymbol{\Gamma}_{\mathrm{L}} - \boldsymbol{D}_{\mathrm{L}}^{\top} \boldsymbol{\Gamma}_{\mathrm{L}} \tilde{\boldsymbol{D}}_{\mathrm{L}}) = \mathrm{col}(\boldsymbol{B}_{\mathrm{L}}^{\top} \tilde{\boldsymbol{B}}_{\mathrm{L}}), \tag{3.33}$$

where $\gamma_{\mathrm{L}} := \mathrm{col}\, \boldsymbol{\Gamma}_{\mathrm{L}}$. The solution of the linear equation (3.33) is

$$\boldsymbol{\Gamma}_{\mathrm{L}} = \begin{pmatrix} 1 & 1 \\ 0 & \frac{1}{15} \end{pmatrix}, \tag{3.34}$$

which has determinant $\frac{1}{15} \neq 0$. With the result (3.34), (3.30) yields

$$\tilde{\boldsymbol{C}}_{\mathrm{L}} = \begin{pmatrix} 1 & 0 \\ -15 & 15 \end{pmatrix}. \tag{3.35}$$

For the right end, a similar transformation

$$\tilde{\Phi}_j^{\mathrm{R}} := \tilde{\boldsymbol{C}}_{\mathrm{R}}\, \tilde{\Phi}_j^{\mathrm{R},\vee} \tag{3.36}$$

is done. In an analogous way, one computes the matrix

$$\boldsymbol{\Gamma}_{\mathrm{R}} = \begin{pmatrix} 1 & 1 \\ -\frac{1}{15} & 0 \end{pmatrix}, \tag{3.37}$$

which also has determinant $\frac{1}{15} \neq 0$, and therefore one gets

$$\tilde{\boldsymbol{C}}_{\mathrm{R}} = \begin{pmatrix} 0 & 1 \\ -15 & 15 \end{pmatrix}. \tag{3.38}$$

The final dual generators are now defined as

$$\tilde{\Phi}_j := \left((\tilde{\Phi}_j^{\mathrm{L}})^{\top}, (\tilde{\Phi}_j^{\mathrm{I}})^{\top}, (\tilde{\Phi}_j^{\mathrm{R}})^{\top}\right)^{\top} \tag{3.39}$$

with $\tilde{\Phi}_j^{\mathrm{L}}$ from (3.28), $\tilde{\Phi}_j^{\mathrm{R}}$ from (3.36). They are plotted in Figure 5.

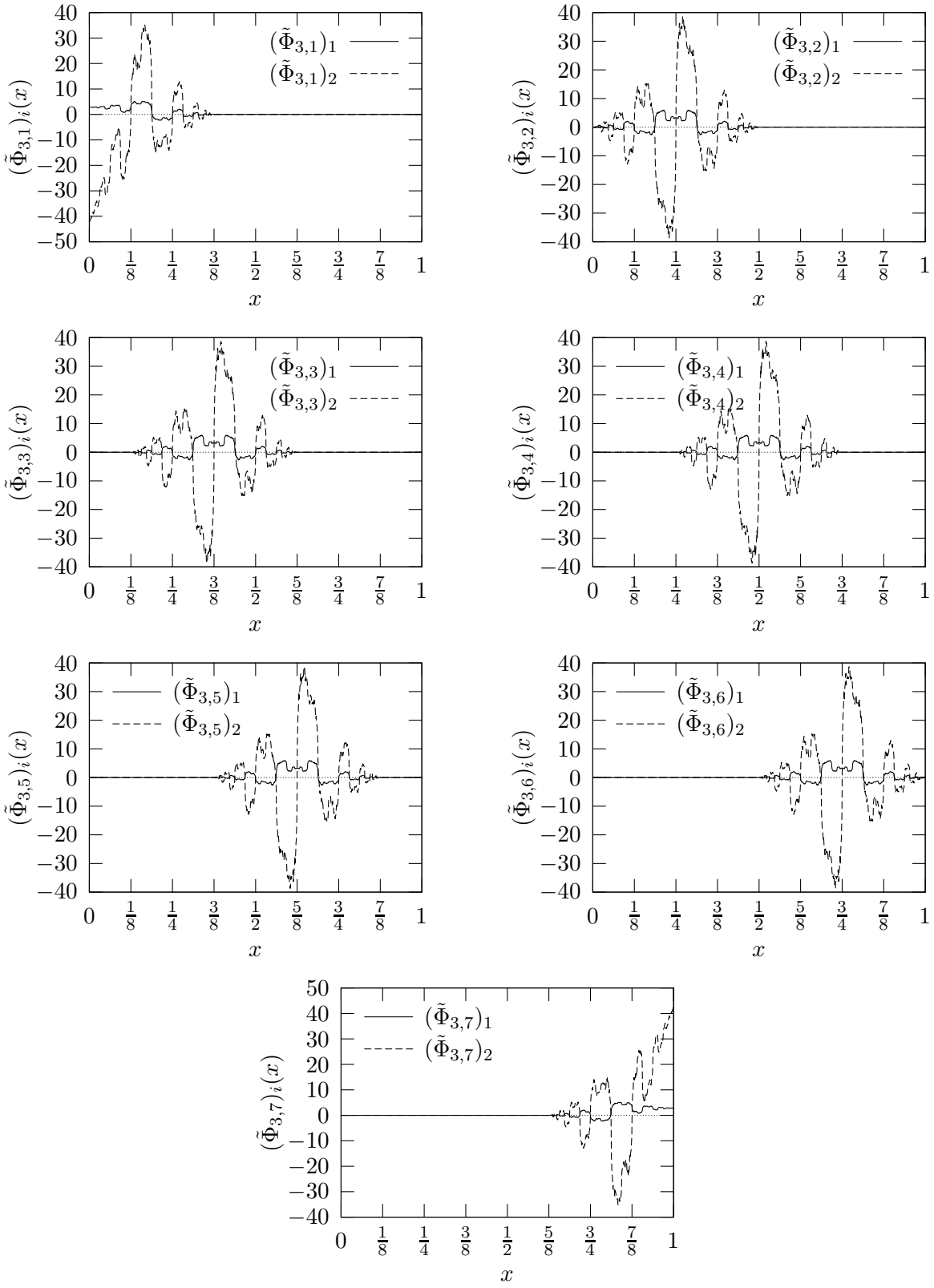

Figure 5: Components of the dual multigenerators $\tilde{\mathbf{\Phi}}_{3,k}, k \in \tilde{\Delta}_3 = \{1, \ldots, 7\}$, on the base level, after biorthogonalization

As the the new dual functions are linear combinations of the preliminary ones, they are still refinable. Now the new refinement matrix is to be derived. Taking into account the transformations (3.28) and (3.36), one gets

$$\tilde{\boldsymbol{M}}_{j,0} = \tilde{\boldsymbol{C}}_{j+1}^{-\top} \tilde{\boldsymbol{M}}_{j,0}^{\vee} \tilde{\boldsymbol{C}}_{j}^{\top} =: \begin{pmatrix} \tilde{\boldsymbol{M}}_{\mathrm{L}} & & \\ & \tilde{\boldsymbol{M}}_{j,0}^{\mathrm{I}} & 0 \\ 0 & & \tilde{\boldsymbol{M}}_{\mathrm{R}} \end{pmatrix} \tag{3.40}$$

with $\tilde{\boldsymbol{C}}_j := \operatorname{diag}(\tilde{\boldsymbol{C}}_{\mathrm{L}}, \mathbf{I}, \tilde{\boldsymbol{C}}_{\mathrm{R}})$ and $\tilde{\boldsymbol{C}}_{\mathrm{L}}, \tilde{\boldsymbol{C}}_{\mathrm{R}}$ from (3.35), (3.38). In particular, $\tilde{\boldsymbol{M}}_{\mathrm{L}}, \tilde{\boldsymbol{M}}_{\mathrm{R}}$ have the form

$$\tilde{\boldsymbol{M}}_{\mathrm{L}} = \begin{pmatrix} \tilde{\boldsymbol{C}}_{\mathrm{L}}^{-\top} \tilde{\boldsymbol{D}}_{\mathrm{L}} \tilde{\boldsymbol{C}}_{\mathrm{L}}^{\top} \\ \tilde{\boldsymbol{B}}_{\mathrm{L}} \tilde{\boldsymbol{C}}_{\mathrm{L}}^{\top} \end{pmatrix} = \frac{1}{\sqrt{2}} \begin{pmatrix} 1 & -\frac{15}{2} \\ 0 & \frac{1}{2} \\ \frac{71}{64} & \frac{123}{128} \\ \frac{5}{64} & \frac{19}{16} \\ \frac{1}{2} & \frac{99}{32} \\ -\frac{3}{16} & -\frac{37}{32} \\ -\frac{7}{64} & -\frac{87}{128} \\ \frac{5}{64} & \frac{31}{64} \end{pmatrix} \in \mathbb{R}^{8\times 2}, \tag{3.41}$$

$$\tilde{\boldsymbol{M}}_{\mathrm{R}} = \begin{pmatrix} \tilde{\boldsymbol{B}}_{\mathrm{R}} \tilde{\boldsymbol{C}}_{\mathrm{R}}^{\top} \\ \tilde{\boldsymbol{C}}_{\mathrm{R}}^{-\top} \tilde{\boldsymbol{D}}_{\mathrm{R}} \tilde{\boldsymbol{C}}_{\mathrm{R}}^{\top} \end{pmatrix} = \frac{1}{\sqrt{2}} \begin{pmatrix} -\frac{7}{64} & \frac{87}{128} \\ -\frac{5}{64} & \frac{31}{64} \\ \frac{1}{2} & -\frac{99}{32} \\ \frac{3}{16} & -\frac{37}{32} \\ \frac{71}{64} & -\frac{123}{128} \\ -\frac{5}{64} & \frac{19}{16} \\ 1 & \frac{15}{2} \\ 0 & \frac{1}{2} \end{pmatrix} \in \mathbb{R}^{8\times 2}. \tag{3.42}$$

Using the notation

$$\mathrm{S}(\Phi_j) := \operatorname{span}\{(\Phi_{j,k})_i : k \in \Delta_j, i \in \{1,2\}\}, \tag{3.43}$$

we summarize the results in the following proposition.

Proposition 3.2. $\mathrm{S}(\Phi_j)$ *and* $\mathrm{S}(\tilde{\Phi}_j)$ *form biorthogonal multiresolution analyses on* $[0,1]$. *The multigenerators are refinable*

$$\Phi_j^{\top} = \Phi_{j+1}^{\top} \boldsymbol{M}_{j,0}, \quad \tilde{\Phi}_j^{\top} = \tilde{\Phi}_{j+1}^{\top} \tilde{\boldsymbol{M}}_{j,0} \tag{3.44}$$

with $\boldsymbol{M}_{j,0}$, $\tilde{\boldsymbol{M}}_{j,0}$ *defined in* (3.20), (3.40). *The support of the generators is*

$$\operatorname{supp} \boldsymbol{\Phi}_{j,k} = 2^{-j}[k-1, k+1], \quad \operatorname{supp} \tilde{\boldsymbol{\Phi}}_{j,k} = 2^{-j}[k-2, k+2] \cap [0,1]. \tag{3.45}$$

In particular, they are locally finite, i. e. with

$$\sigma_{j,k} := \operatorname{supp} \boldsymbol{\Phi}_{j,k}, \quad \tilde{\sigma}_{j,k} := \operatorname{supp} \tilde{\boldsymbol{\Phi}}_{j,k}, \quad k \in \Delta_j$$

we have

$$\begin{aligned} &\#\{k' \in \Delta_j : \sigma_{j,k'} \cap \sigma_{j,k} \neq \varnothing\} \lesssim 1, \quad k \in \Delta_j, \quad j \geq j_0, \\ &\#\{k' \in \tilde{\Delta}_j : \tilde{\sigma}_{j,k'} \cap \tilde{\sigma}_{j,k} \neq \varnothing\} \lesssim 1, \quad k \in \tilde{\Delta}_j, \quad j \geq j_0. \end{aligned} \tag{3.46}$$

Furthermore, $\mathrm{S}(\Phi_j)$ *and* $\mathrm{S}(\tilde{\Phi}_j)$ *have a polynomial exactness of order* $d = 4$ *and* $\tilde{d} = 2$*, respectively.*

4 Multiwavelets on [0, 1]

Given the biorthogonal multigenerators Φ and $\tilde{\Phi}$, we want to construct a set of corresponding biorthogonal multiwavelets Ψ_j and $\tilde{\Psi}_j$, which are bases for the complement spaces of $\mathrm{S}(\Phi_j)$ in $\mathrm{S}(\Phi_{j+1})$ and $\mathrm{S}(\tilde{\Phi}_j)$ in $\mathrm{S}(\tilde{\Phi}_{j+1})$, respectively. For this task the concept of stable completion [CDP96] is used. It is done in two steps: First, in Section 4.1 some *initial* complement is identified. Then, in Section 4.2 this complement basis is projected to a biorthogonal one. The proceeding is similar to the one in [DHJK00].

4.1 An initial stable completion

The task to construct stable multiwavelets for a given multiresolution analysis is equivalent to a matrix extension problem. Thus, for the given matrix $\boldsymbol{M}_{j,0}$ from (3.20) we are looking for a matrix $\boldsymbol{M}_{j,1}^\vee$ such that

$$\boldsymbol{M}_j^\vee := (\boldsymbol{M}_{j,0}, \boldsymbol{M}_{j,1}^\vee) \tag{4.1}$$

is invertible and the inverse is uniformly bounded, i. e.

$$\|\boldsymbol{M}_j^\vee\| = \mathcal{O}(1), \quad \|(\boldsymbol{M}_j^\vee)^{-1}\| = \mathcal{O}(1), \quad j \geq j_0. \tag{4.2}$$

$\boldsymbol{M}_{j,1}^\vee$ is called a *stable completion* of $\boldsymbol{M}_{j,0}$.

One observes that if the generators are interpolatory, then there is a basis of the complement of $S(\Phi_j)$ in $S(\Phi_{j+1})$ given by those functions which interpolate at the grid points $2^{-(j+1)}\Delta_{j+1} \setminus 2^{-j}\Delta_j$, i. e. similar to the construction of hierarchical basis functions. Let

$$\nabla_j := \Delta_{j+1} \setminus \Delta_j = \{2^j, \dots, 2^{j+1} - 1\} \tag{4.3}$$

such that we have $\#\nabla_j = \#\Delta_{j+1} - \#\Delta_j = 2^j$. We define

$$\boldsymbol{\Psi}_{j,k}^\vee := \boldsymbol{\Phi}_{j+1,2k+1-2^{j+1}}, \quad k \in \nabla_j = \{2^j, \dots, 2^{j+1} - 1\} \tag{4.4}$$

and collect the preliminary wavelets in a large vector

$$\Psi_j^\vee := \big((\boldsymbol{\Psi}_{j,2^j}^\vee)^\top, \dots, (\boldsymbol{\Psi}_{j,2^{j+1}-1}^\vee)^\top\big)^\top. \tag{4.5}$$

Then one has

$$(\Psi_j^\vee)^\top = \Phi_{j+1}^\top \boldsymbol{M}_{j,1}^\vee \tag{4.6}$$

with

$$\boldsymbol{M}_{j,1}^{\vee} := \begin{pmatrix} \mathbf{I} & \mathbf{0} & & & & \\ & \mathbf{0} & & & & \\ & \mathbf{I} & \mathbf{0} & & & \\ & & \mathbf{0} & & & \\ & & \mathbf{I} & & & \\ & & & \ddots & & \\ & & & & \mathbf{I} & \mathbf{0} \\ & & & & & \mathbf{0} \\ & & & & & \mathbf{I} \end{pmatrix} \in \mathbb{R}^{2(\Delta_{j+1}\times\nabla_j)} \tag{4.7}$$

and $\mathbf{I}, \mathbf{0} \in \mathbb{R}^{2\times 2}$.

Now we want to check that $\boldsymbol{M}_{j,1}^{\vee}$ is indeed a stable completion. For that purpose one has to check that $\boldsymbol{M}_j^{\vee} = (\boldsymbol{M}_{j,0}, \boldsymbol{M}_{j,1}^{\vee})$ has a uniformly bounded inverse. The existence of

$$(\boldsymbol{M}_j^{\vee})^{-1} =: \boldsymbol{G}_j^{\vee} = \begin{pmatrix} \boldsymbol{G}_{j,0}^{\vee} \\ \boldsymbol{G}_{j,1}^{\vee} \end{pmatrix}$$

is equivalent to the reconstruction formula

$$\Phi_{j+1}^{\top} = \Phi_j^{\top} \boldsymbol{G}_{j,0}^{\vee} + (\Psi_j^{\vee})^{\top} \boldsymbol{G}_{j,1}^{\vee}. \tag{4.8}$$

To show (4.8), we neglect for the moment the boundary blocks in $\boldsymbol{M}_{j,0}$ as they are fixed independent of j. In the interior of the interval, $\boldsymbol{\Phi}_{j,k}$ is refinable with the two-scale relation

$$\boldsymbol{\Phi}_{j,k} = \frac{1}{\sqrt{2}} \sum_{i=-1}^{1} \boldsymbol{A}_i \boldsymbol{\Phi}_{j+1,2k+i} = \frac{1}{\sqrt{2}} \big(\boldsymbol{A}_{-1} \boldsymbol{\Phi}_{j+1,2k-1} + \boldsymbol{A}_0 \boldsymbol{\Phi}_{j+1,2k} + \boldsymbol{A}_1 \boldsymbol{\Phi}_{j+1,2k+1} \big). \tag{4.9}$$

Using the definition (4.4) of the complement functions one gets

$$\boldsymbol{\Phi}_{j,k} = \frac{1}{\sqrt{2}} \big(\boldsymbol{A}_{-1} \boldsymbol{\Psi}_{j,k-1+2^j}^{\vee} + \boldsymbol{A}_0 \boldsymbol{\Phi}_{j+1,2k} + \boldsymbol{A}_1 \boldsymbol{\Psi}_{j,k+2^j}^{\vee} \big).$$

Solving for $\boldsymbol{\Phi}_{j+1,2k}$ yields

$$\boldsymbol{\Phi}_{j+1,2k} = \boldsymbol{A}_0^{-1} \big(\sqrt{2} \boldsymbol{\Phi}_{j,k} - (\boldsymbol{A}_{-1} \boldsymbol{\Psi}_{j,k-1+2^j}^{\vee} + \boldsymbol{A}_1 \boldsymbol{\Psi}_{j,k+2^j}^{\vee}) \big), \tag{4.10}$$

which is of the form (4.8). Recalling that $\boldsymbol{\Phi}_{j+1,2k+1} = \boldsymbol{\Psi}_{j,k+2^j}^{\vee}$, it follows that the inner parts of $\boldsymbol{G}_{j,0}^{\vee}$, $\boldsymbol{G}_{j,1}^{\vee}$ have the form

$$\boldsymbol{G}_{j,0}^{\vee,\mathrm{I}} := \sqrt{2} \begin{pmatrix} \mathbf{0} & \boldsymbol{A}_0^{-1} & \mathbf{0} & & & & & \\ & \mathbf{0} & \mathbf{0} & \boldsymbol{A}_0^{-1} & & & & \\ & & & \mathbf{0} & \mathbf{0} & \boldsymbol{A}_0^{-1} & & \\ & & & & & & \ddots & \\ & & & & & & & \boldsymbol{A}_0^{-1} \\ & & & & & & & \mathbf{0} \end{pmatrix} \tag{4.11}$$

and

$$\boldsymbol{G}_{j,1}^{\vee,\mathrm{I}} := \begin{pmatrix} \mathbf{I} & -(\boldsymbol{A}_0^{-1}\boldsymbol{A}_{-1})^\top & & & & & \\ & -(\boldsymbol{A}_0^{-1}\boldsymbol{A}_1)^\top & \mathbf{I} & -(\boldsymbol{A}_0^{-1}\boldsymbol{A}_{-1})^\top & & & \\ & & & -(\boldsymbol{A}_0^{-1}\boldsymbol{A}_1)^\top \mathbf{I} & & & \\ & & & & \ddots & & \\ & & & & & -(\boldsymbol{A}_0^{-1}\boldsymbol{A}_{-1})^\top & \\ & & & & & -(\boldsymbol{A}_0^{-1}\boldsymbol{A}_1)^\top & \mathbf{I} \end{pmatrix}. \tag{4.12}$$

These matrices have bandwidth independent of j.

To take the boundary effects into account, one computes the product $\boldsymbol{M}_j^\vee \boldsymbol{G}_j^\vee$, which yields

$$\boldsymbol{M}_j^\vee \boldsymbol{G}_j^\vee = \begin{pmatrix} \mathbf{I} & \\ & \boldsymbol{N}_\mathrm{W} \end{pmatrix} =: \boldsymbol{N}_j \tag{4.13}$$

with the wavelet boundary block

$$\boldsymbol{N}_\mathrm{W} = \begin{pmatrix} 1 & 0 & 0 & 0 \\ 0 & 1 & 0 & 0 \\ 0 & \frac{1}{2} & 1 & 0 \\ -\frac{3}{2} & 0 & 0 & 1 \end{pmatrix} \in \mathbb{R}^{4\times 4}, \tag{4.14}$$

independent of j. One checks that $\det \boldsymbol{N}_\mathrm{W} = 1 \neq 0$. By simply multiplying $\boldsymbol{G}_j^\vee$ with the inverse of $\boldsymbol{N}_j$,

$$\boldsymbol{G}_j^{\vee,\mathrm{new}} = \begin{pmatrix} \boldsymbol{G}_{j,0}^{\vee,\mathrm{new}} \\ \boldsymbol{G}_{j,1}^{\vee,\mathrm{new}} \end{pmatrix} := \boldsymbol{G}_j^\vee \boldsymbol{N}_j^{-1}, \tag{4.15}$$

one gets $\boldsymbol{M}_j^\vee \boldsymbol{G}_j^{\vee,\mathrm{new}} = \mathbf{I}$. The boundedness (4.2) follows from the constant bandwith of $\boldsymbol{M}_j^\vee$ and $\boldsymbol{G}_j^{\vee,\mathrm{new}}$. Therefore we have a stable completion.

4.2 Biorthogonal multiwavelets

The above stable completion is not associated with a *biorthogonal* multiwavelet basis. To get biorthogonality, we can apply [CDP96, Corollary 3.1]: The matrices

$$\boldsymbol{M}_{j,1} := (\mathbf{I} - \boldsymbol{M}_{j,0}\tilde{\boldsymbol{M}}_{j,0}^\top)\boldsymbol{M}_{j,1}^\vee \tag{4.16}$$

and

$$\tilde{\boldsymbol{M}}_{j,1} := (\boldsymbol{G}_{j,1}^{\vee,\mathrm{new}})^\top \tag{4.17}$$

are also a stable completion of (3.20), (3.40). They fulfill the biorthogonality relation

$$(\boldsymbol{M}_{j,0}, \boldsymbol{M}_{j,1}) \begin{pmatrix} \tilde{\boldsymbol{M}}_{j,0}^\top \\ \tilde{\boldsymbol{M}}_{j,1}^\top \end{pmatrix} = \mathbf{I}, \tag{4.18}$$

and the inverse $\tilde{\boldsymbol{M}}_j^\top := (\tilde{\boldsymbol{M}}_{j,0}, \tilde{\boldsymbol{M}}_{j,1})^\top$ is uniformly bounded. Furthermore, the primal and dual multigenerators and wavelets

$$\Psi_j := \boldsymbol{M}_{j,1}^\top \Phi_{j+1}, \quad \tilde{\Psi}_j := \tilde{\boldsymbol{M}}_{j,1}^\top \tilde{\Phi}_{j+1} \tag{4.19}$$

form a biorthogonal system,

$$\langle \Psi_j, \tilde{\Psi}_j \rangle_{[0,1]} = \mathbf{I}, \quad \langle \Psi_j, \tilde{\Phi}_j \rangle_{[0,1]} = \langle \Phi_j, \tilde{\Psi}_j \rangle_{[0,1]} = \mathbf{0}. \tag{4.20}$$

The matrix $\boldsymbol{M}_{j,1}$ has the form

$$\boldsymbol{M}_{j,1} = \begin{pmatrix} \boldsymbol{M}_{j,1}^{\mathrm{L}} & & \mathbf{0} \\ & \boldsymbol{M}_{j,1}^{\mathrm{I}} & \\ \mathbf{0} & & \boldsymbol{M}_{j,1}^{\mathrm{R}} \end{pmatrix} \tag{4.21}$$

with

$$\boldsymbol{M}_{j,1}^{\mathrm{L}} := \begin{pmatrix} \frac{9}{32} & \frac{1}{32} \\ -\frac{27}{32} & \frac{33}{32} \\ -\frac{1}{2} & 0 \\ \frac{15}{8} & -\frac{1}{8} \\ \frac{7}{32} & -\frac{1}{32} \\ -\frac{3}{32} & \frac{1}{32} \end{pmatrix} \in \mathbb{R}^{6\times 2}, \qquad \boldsymbol{M}_{j,1}^{\mathrm{R}} := \begin{pmatrix} \frac{7}{32} & \frac{1}{32} \\ \frac{3}{32} & \frac{1}{32} \\ -\frac{1}{2} & 0 \\ -\frac{15}{8} & -\frac{1}{8} \\ \frac{9}{32} & -\frac{1}{32} \\ \frac{27}{32} & \frac{33}{32} \end{pmatrix} \in \mathbb{R}^{6\times 2},$$

and

$$\boldsymbol{M}_{j,1}^{\mathrm{I}} := \begin{pmatrix} \boldsymbol{E}_{\mathrm{I}} & & \\ & \boldsymbol{E}_{\mathrm{I}} & \\ & & \ddots \\ & & & \boldsymbol{E}_{\mathrm{I}} \end{pmatrix}, \qquad \boldsymbol{E}_{\mathrm{I}} := \begin{pmatrix} \frac{35}{512} & -\frac{13}{512} \\ \frac{3}{512} & -\frac{1}{512} \\ -\frac{1}{4} & \frac{3}{32} \\ -\frac{99}{128} & \frac{37}{128} \\ \frac{93}{256} & 0 \\ 0 & \frac{183}{256} \\ -\frac{1}{4} & -\frac{3}{32} \\ \frac{99}{128} & \frac{37}{128} \\ \frac{35}{512} & \frac{13}{512} \\ -\frac{3}{512} & -\frac{1}{512} \end{pmatrix} \in \mathbb{R}^{10\times 2}.$$

The form of the dual matrix $\tilde{\boldsymbol{M}}_{j,1}$ is

$$\tilde{\boldsymbol{M}}_{j,1} = \begin{pmatrix} \mathbf{I}_2 & & & & & & \\ \boldsymbol{G}_{\mathrm{W},1} & \boldsymbol{G}_{\mathrm{W},2} & & & & & \\ & \mathbf{I}_2 & & & & & \\ & \boldsymbol{G}_{\mathrm{W},1} & \boldsymbol{G}_{\mathrm{W},2} & & & & \\ & & & \ddots & & & \\ & & & & \mathbf{I}_2 & & \\ & & & & \boldsymbol{G}_{\mathrm{W},1} & \boldsymbol{G}_{\mathrm{W},2} & \\ & & & & & & \mathbf{I}_2 \end{pmatrix} \tag{4.22}$$

with

$$(\boldsymbol{G}_{\mathrm{W},1}, \boldsymbol{G}_{\mathrm{W},2}) := \begin{pmatrix} -\frac{1}{2} & -\frac{3}{4} & -\frac{1}{2} & \frac{3}{4} \\ \frac{1}{4} & \frac{1}{4} & -\frac{1}{4} & \frac{1}{4} \end{pmatrix} \in \mathbb{R}^{2\times 4}.$$

The wavelets have support

$$\operatorname{supp} \boldsymbol{\Psi}_{j,k} = \operatorname{supp} \tilde{\boldsymbol{\Psi}}_{j,k} = 2^{-j}[k - 2^j - 1, k - 2^j + 2] \cap [0,1]. \tag{4.23}$$

Plots of the primal and dual wavelets on the base level $j = j_0 = 3$ can be found in Figures 6 and 7, respectively. The piecewise polynomial representation of the primal wavelets is

$$(\boldsymbol{\Psi}_{3,8})_1(x) = \begin{cases} -23040\,x^3 + 1728\,x^2, & x \in [0, \frac{1}{16}], \\ 42496\,x^3 - 10560\,x^2 + 768\,x - 16, & x \in [\frac{1}{16}, \frac{1}{8}], \\ 5632\,x^3 - 3648\,x^2 + 768\,x - 52, & x \in [\frac{1}{8}, \frac{1}{4}], \\ 0, & \text{otherwise}, \end{cases}$$

$$(\boldsymbol{\Psi}_{3,8})_2(x) = \begin{cases} 15872\,x^3 - 960\,x^2, & x \in [0, \frac{1}{16}], \\ 15872\,x^3 - 5056\,x^2 + 512\,x - 16, & x \in [\frac{1}{16}, \frac{1}{8}], \\ -512\,x^3 + 320\,x^2 - 64\,x + 4, & x \in [\frac{1}{8}, \frac{1}{4}], \\ 0, & \text{otherwise}, \end{cases}$$

$$(\boldsymbol{\Psi}_{3,9})_1(x) = \begin{cases} -2144\,x^3 + 204\,x^2, & x \in [0, \frac{1}{8}], \\ -32768\,x^3 + 15756\,x^2 - \frac{4905}{2}\,x + \frac{987}{8}, & x \in [\frac{1}{8}, \frac{3}{16}], \\ 32768\,x^3 - 21108\,x^2 + \frac{8919}{2}\,x - \frac{2469}{8}, & x \in [\frac{3}{16}, \frac{1}{4}], \\ +2144\,x^3 - 2208\,x^2 + \frac{1503}{2}\,x - \frac{675}{8}, & x \in [\frac{1}{4}, \frac{3}{8}], \\ 0, & \text{otherwise}, \end{cases}$$

$$(\boldsymbol{\Psi}_{3,9})_2(x) = \begin{cases} 800\,x^3 - 76\,x^2, & x \in [0, \frac{1}{8}], \\ 19520\,x^3 - 8932\,x^2 + \frac{2673}{2}\,x - \frac{261}{4}, & x \in [\frac{1}{8}, \frac{3}{16}], \\ 19520\,x^3 - 13028\,x^2 + \frac{5745}{2}\,x - \frac{837}{4}, & x \in [\frac{3}{16}, \frac{1}{4}], \\ 800\,x^3 - 824\,x^2 + \frac{561}{2}\,x - \frac{63}{2}, & x \in [\frac{1}{4}, \frac{3}{8}], \\ 0, & \text{otherwise}, \end{cases}$$

$$\boldsymbol{\Psi}_{3,k}(x) = \boldsymbol{\Psi}_{3,9}\left(x - \frac{k-9}{8}\right), \quad k \in \{10, \ldots, 14\},$$

$$\boldsymbol{\Psi}_{3,15}(x) = \boldsymbol{J}\,\boldsymbol{\Psi}_{3,8}(1-x).$$

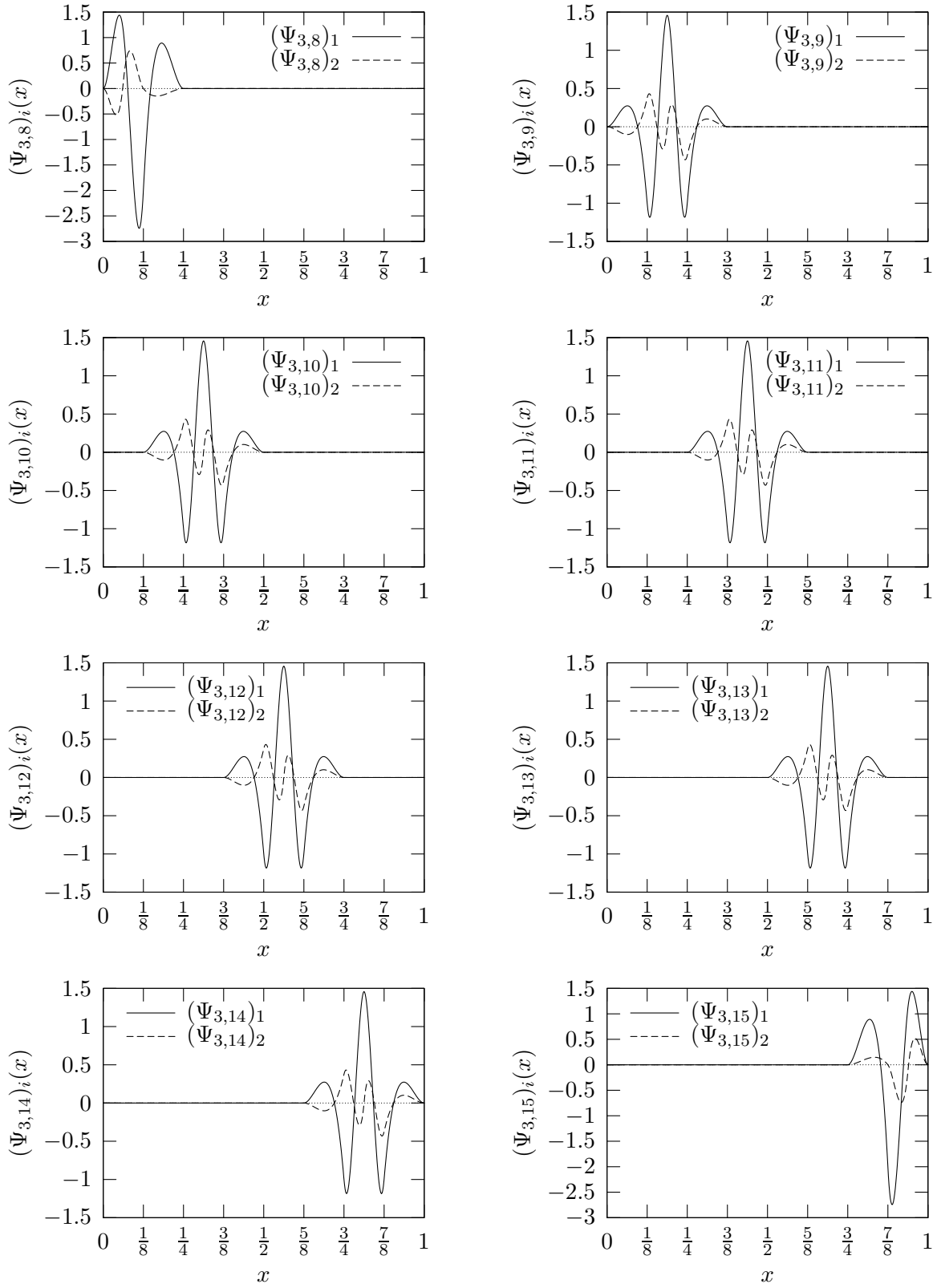

Figure 6: Components of the primal multiwavelets $\Psi_{3,k}, k \in \nabla_3 = \{8, \ldots, 15\}$, on the base level

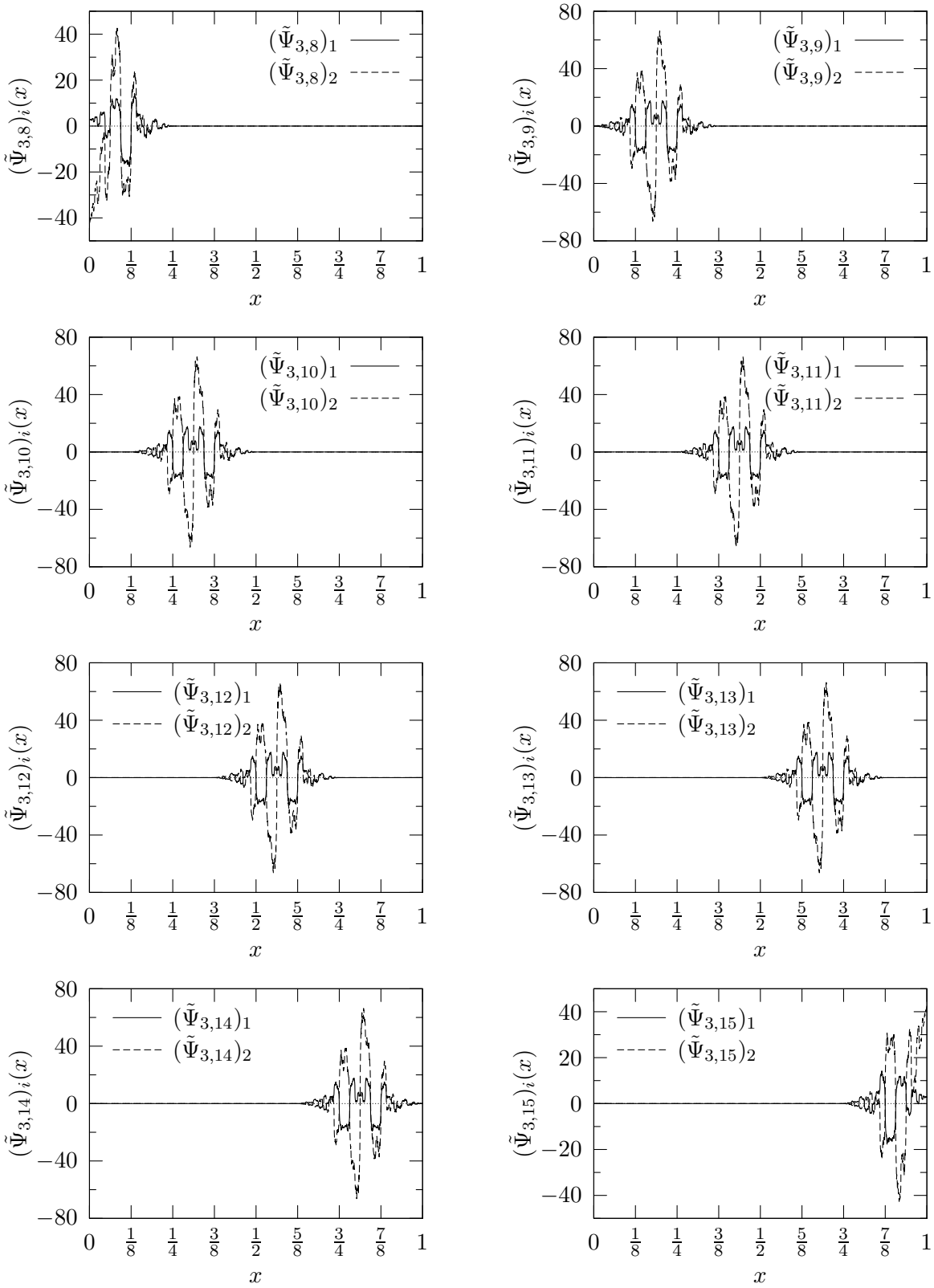

Figure 7: Components of the dual multiwavelets $\tilde{\Psi}_{3,k}, k \in \tilde{\nabla}_3 = \{8, \ldots, 15\}$, on the base level

5 Numerical results

As stated in the introduction, the initial motivation for the multiwavelet basis constructed in Sections 2–4 is the application to the numerical discretization of operator equations. In this section, we summarize the numerical results obtained so far. These show the superiority of the new construction in comparison to existing ones for elliptic equations with homogeneous Dirichlet boundary conditions of second order.

5.1 Determination of the L_2 Riesz constants.

In order to analyze the L_2-stability of the basis, the Riesz constants have been computed numerically. Following [Pri06, Chapter 6], with the Gramian matrix $\boldsymbol{G} = (\langle \psi_\lambda, \psi_\mu \rangle_{L_2})_{\lambda,\mu\in\Lambda}$ we have

$$C_1 = \sqrt{\lambda_{\min}(\boldsymbol{G})}, \qquad C_2 = \sqrt{\lambda_{\max}(\boldsymbol{G})},$$

where $\lambda_{\max}(\boldsymbol{A})$ is the largest and $\lambda_{\min}(\boldsymbol{A})$ the smallest eigenvalue of a matrix $\boldsymbol{A}$. These values are numerically calculated for finite submatrices $\boldsymbol{G}_j = (\langle \psi_\lambda, \psi_\mu \rangle_{L_2})_{\lambda,\mu\in\Lambda_j}$, $\Lambda_j := \Delta_{j_0} \cup \bigcup_{\ell=j_0}^{j-1} \nabla_\ell$, which belong to the spaces $\mathrm{S}(\Phi_j)$. The Riesz constants $C_1^{(j)}, C_2^{(j)}$ of the subspaces $\mathrm{S}(\Phi_j)$ converge to the Riesz constants C_1, C_2 of the full basis for $j \to \infty$. Since the components of the actual multiwavelet basis have different L_2 norms, the diagonal preconditioner $\boldsymbol{D}_j = \mathrm{diag}(\|\psi_\lambda\|_{L_2})_{\lambda\in\Lambda_j}$ is applied to the matrix $\boldsymbol{G}_j$. This is equivalent to a component-wise L_2 normalization of the wavelet functions and effects an improvement of stability. The results are shown in Table 2 and Figure 8. For a comparison, the condition numbers of the Gramian matrices $\kappa(\boldsymbol{G}_j) =$

j	$C_1^{(j)}$	$C_2^{(j)}$	$\kappa(\boldsymbol{G}_j)$
3	0.410046	1.55090	14.3054
4	0.341071	1.71910	25.4047
5	0.310167	1.80281	33.7837
6	0.292832	1.87020	40.7885
7	0.282015	1.91160	45.9461
8	0.274721	1.93933	49.8332
9	0.269484	1.95816	52.7996
10	0.265521	1.97171	55.1427
11	0.262392	1.98167	57.0378
12	0.259840	1.98925	58.6093
13	0.257707	1.99512	59.9358
14	0.255893	1.99978	61.0724
15	0.254330	2.00352	62.0571
16	0.252970	2.00658	62.9176
17	0.251779	2.00910	63.6741

Table 2: Numerical results for the Riesz constants of the L_2-normalized basis

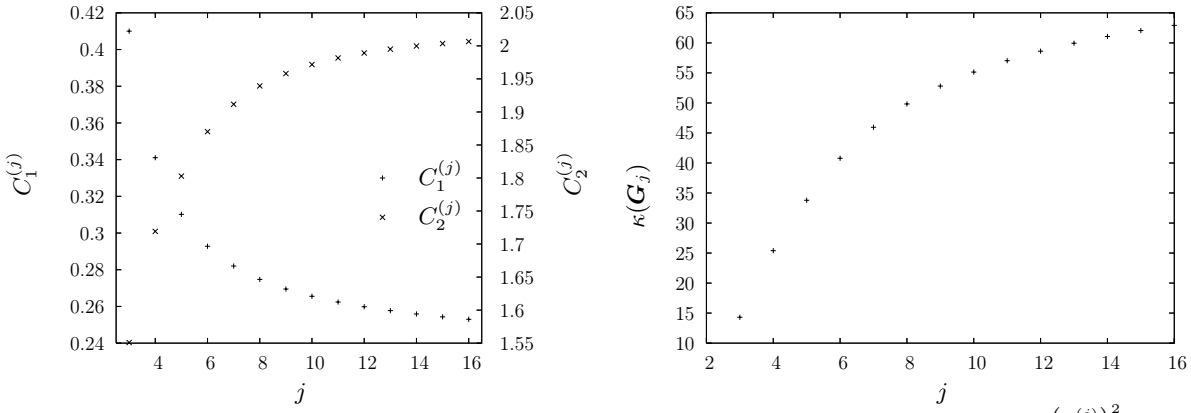

(a) Riesz constants $C_1^{(j)}$, $C_2^{(j)}$

(b) Condition number $\kappa(\boldsymbol{G}_j) = \frac{\left(C_2^{(j)}\right)^2}{\left(C_1^{(j)}\right)^2}$

Figure 8: Numerical results for the Riesz constants

$(C_2^{(j)})^2/(C_1^{(j)})^2$ have also been computed for the bases from [Pri06] (with spline order $d = 4$, $\tilde{d} = 4$ which also has 4 vanishing moments) and [DS98] (with $d = 4$, $\tilde{d} = 4$ and the Bernstein biorthogonalization method), see Table 3 and Figure 9.

For classical wavelets there is a theorem by K. Bittner ([Bit05, Theorem 6]) which gives the

j	S.	[Pri06]	[DS98]
3	14.3054	—	—
4	25.4047	70.5141	—
5	33.7837	146.147	1876.4
6	40.7885	260.003	11468.2
7	45.9461	387.202	27451.2
8	49.8332	517.511	39891.6
9	52.7996	651.858	54601.1
10	55.1427	794.031	66108.0
11	57.0378	1059.11	81841.1
12	58.6093	1490.99	92186.1
13	59.9358	2007.91	100521
14	61.0724	2724.97	101650
15	62.0571	3567.77	104678
16	62.9176	4799.46	102613
17	63.6741	5440.93	108236

Table 3: Condition numbers of the Gramian matrices for different constructions

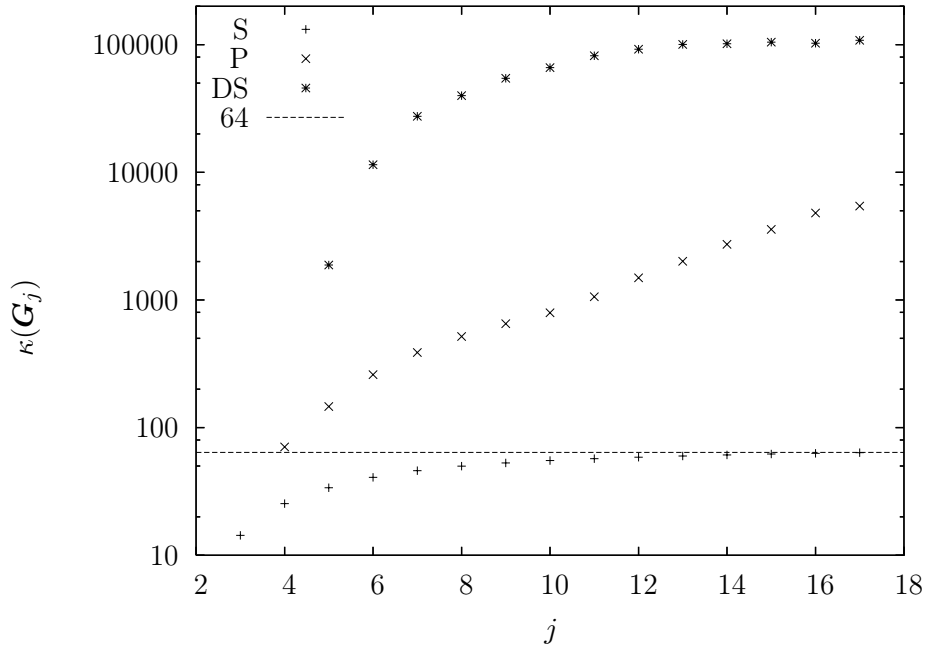

Figure 9: Condition numbers of the Gramian matrices for different bases

lower bound

$$\kappa(\boldsymbol{G}) = \frac{C_2^2}{C_1^2} \geq 4^{d-1} \tag{5.1}$$

for the quotient of the Riesz constants, where d is the (primal) polynomial order. Although it has not yet been rigorously proved, we also expect the theorem to hold for the case of multiwavelets, and indeed, in our experiment the values of $\kappa(\boldsymbol{G}_j)$ approach the minimal value of $2^{4-1} = 64$ which would be predicted for a classical wavelet basis. This indicates that the construction is almost optimal.

5.2 Wavelet Galerkin scheme

As a test problem, the biharmonic equation is used which will be now defined. Let $\Delta := \sum_{k=1}^{n} \frac{\partial^2}{\partial x_k^2}$ be the Laplace operator. The biharmonic equation with homogeneous Dirichlet boundary conditions on a domain $\Omega \subset \mathbb{R}^n$ is defined as

$$\Delta^2 u = g \quad \text{on } \Omega, \qquad u = \frac{\partial u}{\partial n} = 0 \quad \text{on } \partial\Omega. \tag{5.2}$$

With the bilinear form

$$a : H_0^2(\Omega) \times H_0^2(\Omega) \to \mathbb{R}, \quad a(u,v) := \int_\Omega (\Delta u)(x)\,(\Delta v)(x)\,\mathrm{d}x \tag{5.3}$$

and the right hand side

$$f : H_0^2(\Omega) \to \mathbb{R}, \quad f(v) := \int_\Omega g(x)\,v(x)\,\mathrm{d}x, \tag{5.4}$$

the weak formulation of (5.2) is: Find a $u \in H_0^2(\Omega)$, such that

$$a(u, v) = f(v) \quad \text{for all } v \in H_0^2(\Omega). \tag{5.5}$$

As a first numerical test of the wavelet basis, the one-dimensional biharmonic equation (5.2) with the constant right hand side $g \equiv 384$ is considered. The exact solution is the smooth function $u(x) = 16\,x^2\,(1-x)^2$, see Figure 10. For the discretization a wavelet Galerkin scheme with $\mathrm{S}(\Phi_j)$ as ansatz space has been chosen. As the scaled wavelet basis $\{2^{-2|\lambda|}\psi_\lambda : \lambda \in \Lambda\}$ is a Riesz basis in the energy space H_0^2, the convergence of the Galerkin solution u_j to the exact solution u for $j \to \infty$ is assured. This fact also causes the spectral condition number $\kappa(\boldsymbol{A}_j)$ of the stiffness matrix $\boldsymbol{A}_j := (a(\psi_\lambda, \psi_\mu))_{\lambda,\mu\in\Lambda_j} = (\langle\psi''_\lambda, \psi''_\mu\rangle)_{\lambda,\mu\in\Lambda_j}$ to be bounded. The condition number $\kappa(\boldsymbol{A}_j)$ has been calculated for various j. For a comparison, this computation has also been carried out with the basis from [Pri06] (again with spline order $d = 4$, $\tilde{d} = 4$) and the basis from [DS98] ($d = 4$, $\tilde{d} = 4$, Bernstein biorthogonalization method). The results are shown in Table 4 and they are visualized in Figure 11 (the figure does not contain the data from [DS98] because they are in another order of magnitude).

Also, the global discretization error has been computed on a dyadic grid with resolution 15 (i. e. with $2^{15} + 1$ points). From this the global L_∞ error was determined, as well as the L_2 error and the H^2 error, where numerical integration (a composite trapezoidal rule) and for the latter one numerical differentiation was used. The results can be seen in Table 5 and in Figure 12.

To determine the realized convergence order, a data fit with the ansatz $y = a\,2^{-pj}$ has been made in form of a linear regression with the data $(j, \log_2 y)$. For the L_∞ error we have an order of $p_{L_\infty} = 4$, for the L_2 error $p_{L_2} = 4.04255$ and for the H^2 error $p_{H^2} = 2.03025$. This is very near to the theoretical values. The Jackson inequality and Céa's lemma yields $p_{H^2} = 2$. For the L_2 error one gets a theoretical convergence rate of $p_{L_2} = 4$ via an Aubin-Nitsche trick.

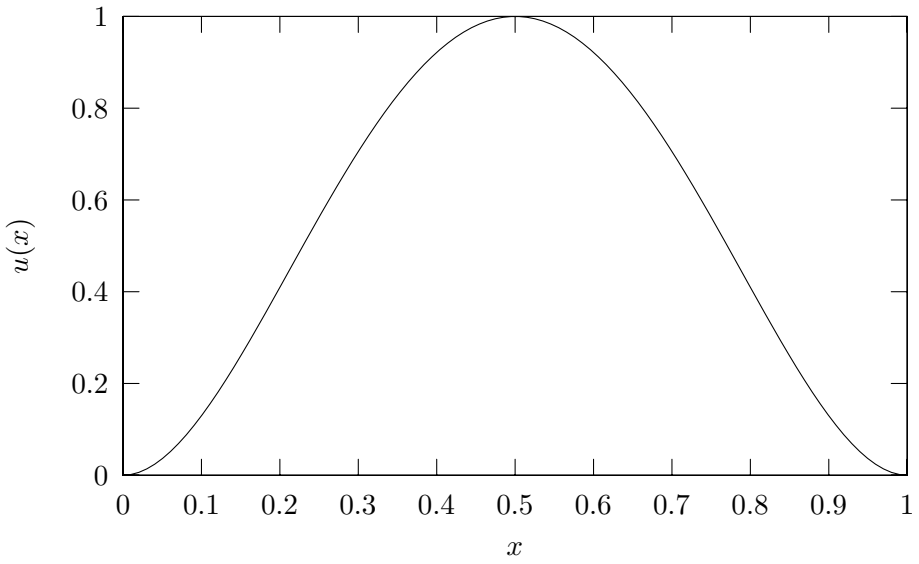

Figure 10: Exact solution $u(x) = 16\,x^2\,(1-x)^2$ of the one-dimensional biharmonic equation (5.2) with constant right hand side

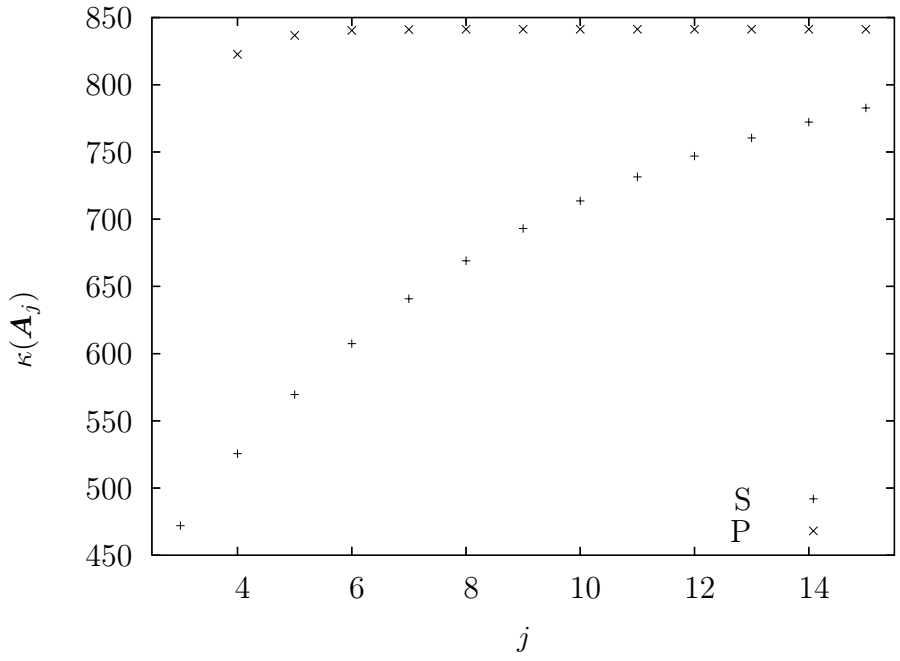

Figure 11: Condition number of the stiffness matrix $\boldsymbol{A}_j$ of the biharmonic equation for different bases

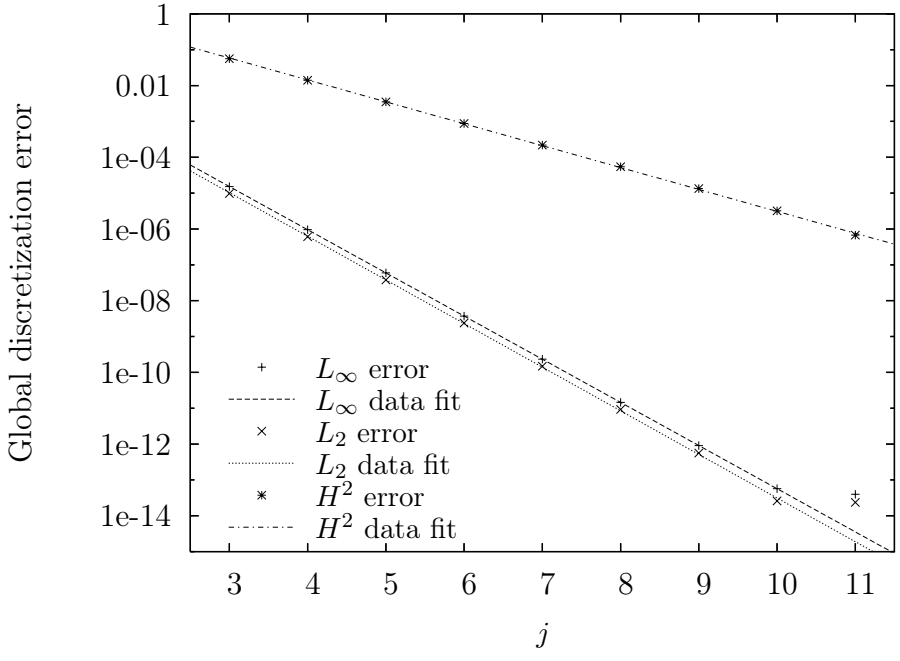

Figure 12: Global discretization error for the solution of the biharmonic equation for several ansatz spaces $\mathrm{S}(\Phi_j)$

j	S.	[Pri06]	[DS98]
3	471.989	—	—
4	525.580	822.621	—
5	569.547	836.704	17037.7
6	607.451	840.349	17047.2
7	640.800	841.067	20521.2
8	669.000	841.234	24923.3
9	693.022	841.271	27620.9
10	713.628	841.279	29337.7
11	731.420	841.281	30238.3
12	746.877	841.281	30999.8
13	760.380	841.281	31322.4
14	772.237	841.281	32087.1
15	782.702	841.281	32203.3

Table 4: Condition number of the stiffness matrix $\boldsymbol{A}_j$ of the biharmonic equation for different bases

j	$\kappa(\boldsymbol{A}_j)$	L_∞ error	L_2 error	H^2 error
3	471.989	1.52588e−05	9.72665e−06	5.64459e−02
4	525.580	9.53674e−07	6.07915e−07	1.40421e−02
5	569.547	5.96046e−08	3.79947e−08	3.50179e−03
6	607.451	3.72529e−09	2.37465e−09	8.74191e−04
7	640.800	2.32831e−10	1.48399e−10	2.18223e−04
8	669.000	1.45519e−11	9.25873e−12	5.43518e−05
9	693.022	9.09495e−13	5.62641e−13	1.34093e−05
10	713.628	5.68434e−14	2.60047e−14	3.19476e−06
11	731.420	3.96350e−14	2.35827e−14	6.70521e−07

Table 5: Condition number of the stiffness matrix and discretization error for the biharmonic equation

5.3 Adaptive wavelet frame scheme

In this subsection, we want to use an adaptive wavelet frame scheme [DFR$^+$07] to solve the operator equation (5.2). The intention is to show that using the basis introduced in this paper as starting point for the construction of the frame leads to better numerical results.

The concept of frames and a method to construct wavelet frames on a domain will now be shortly recalled. A frame $\mathcal{F}$ in a Hilbert space $\mathcal{H}$ is a sequence $\mathcal{F} = (\psi_\lambda)_{\lambda\in\Lambda}$ with the index set

Λ where there exist constants $C_1, C_2 > 0$ such that

$$C_1\|f\|_{\mathcal{H}}^2 \leq \sum_{\lambda\in\Lambda} |\langle f, \psi_\lambda\rangle_{\mathcal{H}}|^2 \leq C_2\|f\|_{\mathcal{H}}^2 \quad \text{for all } f \in \mathcal{H} \tag{5.6}$$

holds. In particular, every Riesz basis for $\mathcal{H}$ is also a frame for $\mathcal{H}$.

In order to discretize an elliptic problem $\mathcal{L}u = f, \mathcal{L} : H_0^t(\Omega) \to H^{-t}(\Omega)$, a frame which characterizes the solution space $H^t(\Omega)$, i. e., which satisfies

$$\|f\|_{H^t(\Omega)} \eqsim \left(\sum_{\lambda\in\Lambda} 2^{2|\lambda|t} |\langle f, \tilde{\psi}_\lambda\rangle_{L_2(\Omega)}|^2\right)^{1/2} \quad \text{for } f \in H_0^t(\Omega), \tag{5.7}$$

is needed. This is satisfied by Gelfand frames which will now be defined. The weighted ℓ_p space $\ell_{p,w}(\Lambda)$ on the countable index set Λ with respect to the weight $w : \Lambda \to \Lambda$ is induced by the norm

$$\|\boldsymbol{c}\|_{\ell_{p,w}(\Lambda)} := \left(\sum_{\lambda\in\Lambda} |c_\lambda|^p\, w(\lambda)^p\right)^{1/p}. \tag{5.8}$$

A frame $\mathcal{F}$ for $L_2(\Omega)$ is called a Gelfand frame for $(H_0^t(\Omega), L_2(\Omega), H^{-t}(\Omega))$, if $\mathcal{F} \subset H_0^t(\Omega)$, if we have for the canonical dual frame $\tilde{\mathcal{F}} \subset H^{-t}(\Omega)$, and if the analysis operator and the synthesis operator

$$\tilde{F} : H^t \to \ell_{2,2^t}(\Lambda), \quad f \mapsto \left(\langle f, \tilde{\psi}_\lambda\rangle_{L_2(\Omega)}\right)_{\lambda\in\Lambda} \quad \text{and} \quad F^* : \ell_{2,2^t}(\Lambda) \to H^t, \quad \boldsymbol{c} \mapsto \sum_{\lambda\in\Lambda} c_\lambda\, \psi_\lambda \tag{5.9}$$

are both well-defined and bounded. The spaces $(H_0^t(\Omega), L_2(\Omega), H^{-t}(\Omega))$ form a Gelfand triple, i. e. $H^t(\Omega) \subset L_2(\Omega) \eqsim (L_2(\Omega))' \subset H^{-t}(\Omega)$ with continuous and dense embeddings. Between the sequence spaces we have the isomorphisms $D : \ell_{2,2^t}(\Lambda) \to \ell_2(\Lambda), c_\lambda \mapsto 2^{|\lambda|t} c_\lambda$ and $D^* : \ell_2(\Lambda) \to \ell_{2,2^t}(\Lambda)', c_\lambda \mapsto 2^{-|\lambda|t} c_\lambda$.

A wavelet Gelfand frame for $(H_0^t(\Omega), L_2(\Omega), H^{-t}(\Omega))$ can be constructed as a union of wavelet bases on subdomains $\Omega_i \subset \Omega$ which cover Ω, i. e. $\bigcup_i \Omega_i = \Omega$ [Ste03, DFR06]. On each patch Ω_i, the corresponding wavelet basis is the parametric image of a basis on the unit cube $[0,1]^n$. This cube basis is in turn a tensor product of bases on the interval $[0,1]$.

How we can use such frames to solve PDEs is shown in the following lemma [DFR06, Lemma 4.1].

Lemma 5.1. *The operator*

$$\boldsymbol{G} := (D^*)^{-1} F \mathcal{L} F^* D^{-1} \tag{5.10}$$

is a bounded operator from $\ell_2(\Lambda)$ to $\ell_2(\Lambda)$. Moreover, $\boldsymbol{G} = \boldsymbol{G}^*$ and it is boundedly invertible on its range $\operatorname{ran}(\boldsymbol{G}) = \operatorname{ran}((D^*)^{-1}F)$.

From this lemma one obtains that (5.2) is equivalent to the (infinite) system of equations

$$\boldsymbol{G}\boldsymbol{u} = \boldsymbol{f}. \tag{5.11}$$

The solution u of the PDE then can be regained via

$$u = F^* D^{-1} \boldsymbol{u}. \tag{5.12}$$

Thus we are left to find an algorithm for approximating such a linear system of equations. It is shown in [Ste03, DFR06, DFR$^+$07] that the well-known iterative schemes for finite dimensional linear systems of equations, the damped Richardson iteration and steepest descent, also converge in the infinite dimensional case. To get an implementable version, a finite iteration vector $\boldsymbol{u}_k$ is used, and the right-hand side $\boldsymbol{f}$ and the matrix-vector product $\boldsymbol{u}_k \mapsto \boldsymbol{G}\boldsymbol{u}_k$ are replaced by finite dimensional approximations. The latter is enabled by the compressibility of the system matrix $\boldsymbol{G}$, i. e. the coefficients decay exponentially with the distance to the main diagonal. Therefore the required columns of $\boldsymbol{G}$ can be thinned out adaptively, such that the result of the approximated matrix vector multiplication equals the exact one up to a given accuracy. The complexity of such a method is linear in the length of the input vector $\boldsymbol{u}_k$.

The theoretical convergence order of an adaptive wavelet or frame method depends on the Besov regularity of the exact solution [Coh03, DFP$^+$07]. If n is the space dimension, t the Sobolev smoothness of the frame and d the order of (primal) polynomial reproduction, it holds that if $u \in B_\tau^{sn+t}(L_\tau(\Omega))$ for $0 < s < \frac{d-t}{n}$ and $\tau = (s+\frac{1}{2})^{-1}$, then $\|\boldsymbol{u} - \boldsymbol{u}_k\|_{\ell_2(\Lambda)} \lesssim (\operatorname{supp} \boldsymbol{u}_k)^{-s}$. In particular, the best convergence rate is

$$\frac{d-t}{n}, \tag{5.13}$$

see [Ste03, Section 4.2], [DFP$^+$07] for details.

For the test problem we chose an exact solution which is a sum of a smooth part

$$u_{\mathrm{reg}}(x) = -\cos(2\pi x) + 1 \tag{5.14}$$

and a singular part

$$u_{\mathrm{sing}}(x) = \begin{cases} 48\,x^4 - 63\,x^3 + \frac{47}{2}\,x^2, & x \in [0, \frac{1}{2}], \\ 48\,x^4 - 127\,x^3 + \frac{235}{2}\,x^2 - 46\,x + \frac{15}{2}, & x \in [\frac{1}{2}, 1] \end{cases} \tag{5.15}$$

which is C^1 but not C^2. Therefore, the Sobolev regularity of the exact solution is small, $u \in H^{5/2}$, but $u \in B_\tau^s(L_\tau(\Omega))$ for all $s > 0$ where $\frac{1}{\tau} = s - \frac{3}{2}$, since u_{sing} is piecewise analytic. The function u is plotted in Figure 13. The corresponding right hand side for the weak formulation is

$$f(v) = 4\,v'\left(\frac{1}{2}\right) - 384\,v\left(\frac{1}{2}\right) - 16\int_0^1 \left(\pi^4 \cos(2\pi x) - 72\right) v(x)\,\mathrm{d}x. \tag{5.16}$$

An adaptive steepest descent algorithm [DFR$^+$07] has been used to discretize this problem. For the overlapping open covering $(0, 0.7) \cup (0.3, 1)$, aggregated wavelet frames have been constructed, where different bases have been used. Here, according to (5.13), we have an optimal rate of $\frac{4-2}{1} = 2$. Figure 14 shows a logarithmic plot of the realized convergence order for the basis introduced in this paper (S) and the basis from [Pri06] with $d = 4$, $\tilde{d} = 4$ (P). The optimal rate of 2 is indicated as straight line. As can be seen in the figure, the basis from this paper realizes the optimal convergence rate. With the basis from [Pri06], only a convergence rate of 1 could be obtained, probably due to stability problems of the basis.

Acknowledgments

The author would like to thank Thorsten Raasch and Manuel Werner for their helpful suggestions and acknowledges the financial support provided by the DFG under grant Da 360/4-3.

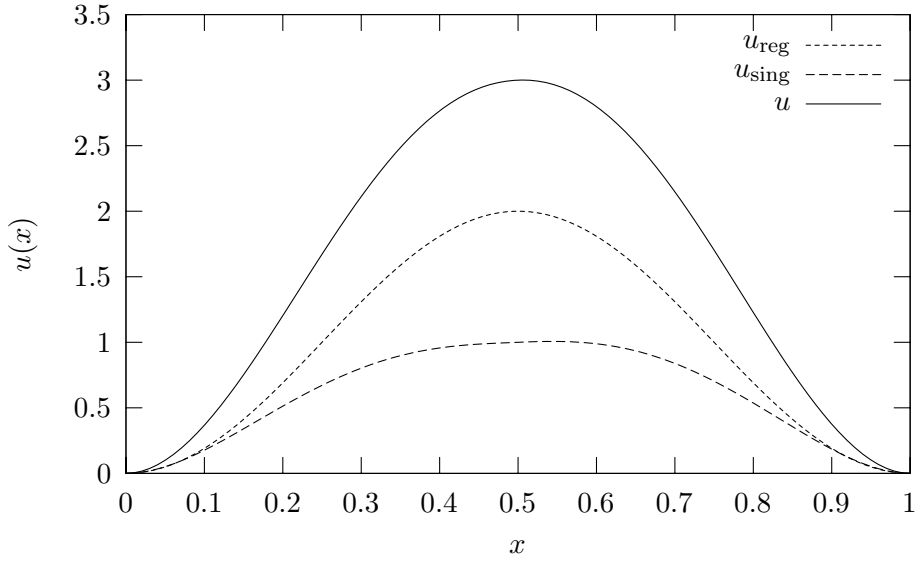

Figure 13: Exact solution of the one-dimensional biharmonic equation (5.2) with the right hand side (5.16)

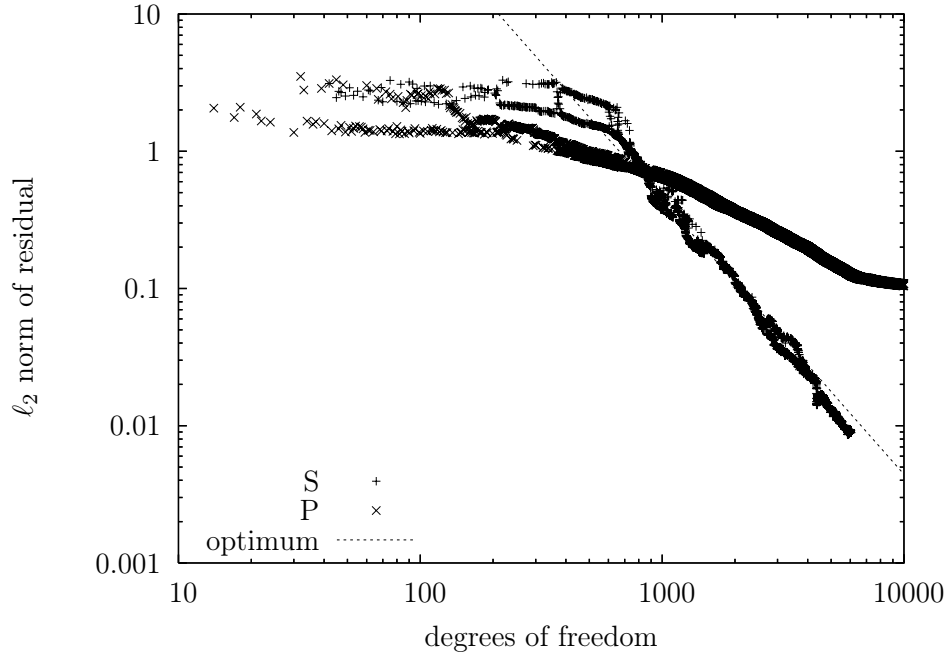

Figure 14: ℓ_2 norm of the residual versus number of active frame elements for a steepest descent scheme with aggregated wavelet frames constructed from different bases. S marks the basis published in this paper, P the basis from [Pri06].

References

[Bit05] Kai Bittner, *A new view on biorthogonal spline wavelets*, Preprint, Universität Ulm, 2005.

[CDP96] Jesús M. Carnicer, Wolfgang Dahmen, and Juan Manuel Peña, *Local decomposition of refinable spaces and wavelets*, Applied and Computational Harmonic Analysis **3** (1996), no. 2, 127–153.

[Coh03] Albert Cohen, *Numerical analysis of wavelet methods*, Studies in Mathematics and its Applications, vol. 32, North-Holland, Amsterdam, 2003.

[DFP+07] Stephan Dahlke, Massimo Fornasier, Miriam Primbs, Thorsten Raasch, and Manuel Werner, *Nonlinear approximation with Gelfand frames*, in preparation.

[DFR06] Stephan Dahlke, Massimo Fornasier, and Thorsten Raasch, *Adaptive frame methods for elliptic operator equations*, Advances in Computational Mathematics (2006), published online, DOI 10.1007/s10444-005-7501-6.

[DFR+07] Stephan Dahlke, Massimo Fornasier, Thorsten Raasch, Rob Stevenson, and Manuel Werner, *Adaptive frame methods for elliptic operator equations: The steepest descent approach*, IMA Journal of Numerical Analysis (2007), published online, DOI 10.1093/imanum/drl035.

[DHJK00] Wolfgang Dahmen, Bin Han, Rong-Qing Jia, and Angela Kunoth, *Biorthogonal multiwavelets on the interval: Cubic Hermite splines*, Constructive Approximation **16** (2000), no. 2, 221–259.

[DKU99] Wolfgang Dahmen, Angela Kunoth, and Karsten Urban, *Biorthogonal spline wavelets on the interval—stability and moment conditions*, Applied and Computational Harmonic Analysis **6** (1999), no. 2, 132–196.

[DS98] Wolfgang Dahmen and Reinhold Schneider, *Wavelets with complementary boundary conditions – Function spaces on the cube*, Results in Mathematics **34** (1998), no. 3–4, 255–293.

[Pri06] Miriam Primbs, *Stabile biorthogonale Spline-Waveletbasen auf dem Intervall*, Dissertation, Universität Duisburg-Essen, 2006.

[Ste03] Rob Stevenson, *Adaptive solution of operator equations using wavelet frames*, SIAM Journal on Numerical Analysis **41** (2003), no. 3, 1074–1100.